Waste and Biomass Valorization
https://doi.org/10.1007/s12649-026-03603-1

ORIGINAL PAPER

Preliminary Investigation of a Lignin-Based Hydrogel for the Removal of Metal Corrosion Products from Stones

Valeria Stagno[1,2] · Melania Di Fazio[1] · Laura Giuliani[1] · Rosaceleste Zumpano[3] · Alessandro Ciccola[4] · Elisa Villani[1] · Chiara Genova[2] · Laura Medeghini[1] · Silvia Capuani[2]

Received: 17 October 2025 / Accepted: 1 April 2026

Abstract

Lignin is a major constituent of the plant biomass, on top of agricultural waste, and a by-product of the paper industry. At present, most waste lignin is burned for energy recovery, whereas only a limited fraction is exploited in industrial recycling processes. In the context of circular economy strategies and sustainable waste valorisation, lignin can be converted into advanced materials, such as hydrogels. Lignin-based hydrogels can serve as absorbents for heavy metal ions due to the negatively charged oxygens of lignin functional groups. These materials are currently employed as drug delivery systems, in water remediation, and as sensors. In this study, lignin is valorised through its conversion into nanoparticles embedded in a PVA–borax matrix and proposed for an innovative application: the cleaning of metal-contaminated stone artworks. Three lithotypes (Candoglia marble, Carrara marble, and travertine) were artificially contaminated with metal corrosion products and subsequently cleaned using the lignin-based hydrogel. The cleaning performance was evaluated directly on the stone surface by using a non-invasive approach based on portable Fourier Transform Infrared (FTIR) spectroscopy, single-sided Nuclear Magnetic Resonance (NMR) relaxometry and colorimetric analyses. In addition, Attenuated Total Reflectance FTIR (ATR-FTIR) spectroscopy was employed to characterize the corrosion products and the lignin-based hydrogel and elucidate lignin–metal interactions. Preliminary results suggest that the cleaning performance depends on the petrophysical properties of the stone substrate and on the nature of the contaminants. A synergistic contribution of the hydrogel components to the cleaning process was also observed.

Extended author information available on the last page of the article

Published online: 28 April 2026

Graphical Abstract

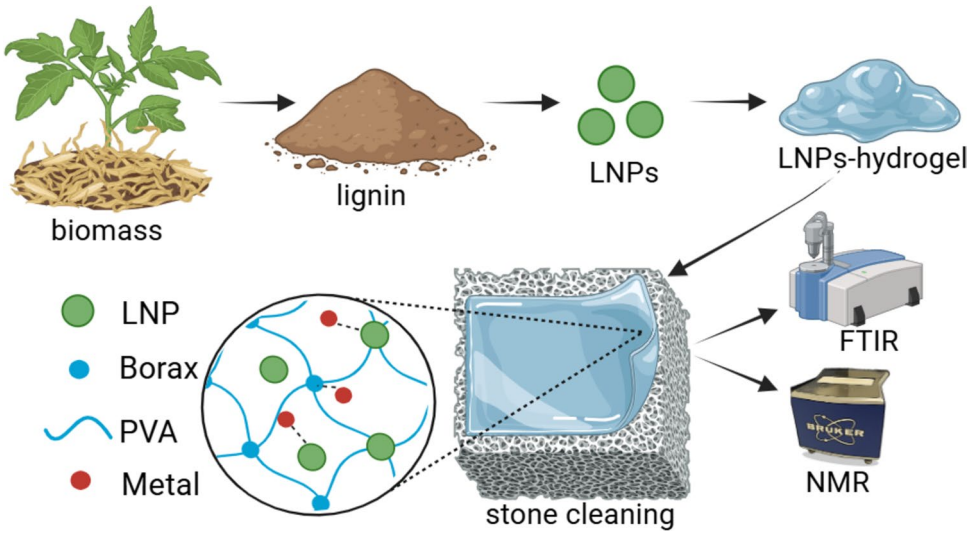

Keywords Lignin valorisation · Lignin-based hydrogel · Stones conservation · Portable FTIR · Portable NMR · Circular economy

Introduction

In recent years, the interest in converting waste into high-value-added products has increased [1–3]. Lignocellulosic biomass is on top of agricultural waste, which is often burned to generate energy [4–6]. Moreover, this waste biomass is also produced as forestry residues obtained from cleaning, thinning, or final felling of a forest, from secondary production operations and industries, such as sawmills and timber processing units [7–9]. These by-products have limited heat output and economic value; therefore, transporting these potential fuel sources from rural to urban areas is expensive [9]. The major constituents of the residues obtained from agricultural waste include different proportions of hemicellulose (25–50%), cellulose (37–50%), and lignin (5–15%), compared to forest residues, made of cellulose (34–54%), hemicellulose (19–34%), lignin (11–30%) and others (3–6%) [9–11]. Conversely, the plant biomass consists of 40–45 wt% of cellulose, 25–35 wt% of hemicellulose, 15–30 wt% of lignin, and inorganic materials [12]. Among the three, only lignin is considered inexpensive, and 98% is burned to generate energy, whereas the remaining 2% is used in the manufacture of livestock feed, vanillin, fillers in cements, in the manufacture of carbon fibers, as well as a complement in agglomerates and adhesives [1, 13–16]. Lignin is also an important by-product of the paper industry that mainly exploits wood as raw material [1].Considering that lignin is linked to other wood constituents (i.e., hemicellulose, cellulose), enzymatic, chemical, and mechanical processes are used to extract it. The different processes produce different types of lignins [1, 17–23], for example, alkali lignin (used in this work), which is mainly obtained from the kraft process, hydrolytic lignin obtained by enzymatic hydrolysis, organosolv lignin by the organosolv process, and lignosulfonates obtained by the sulfite process.

Lignin is an amorphous biomacromolecule with a molecular mass ranging from 1000 to 20,000 g/mol. Although it is not a defined structure, lignin is mainly composed of repeated units, such as three different monomers called sinapyl alcohol, coniferyl alcohol, and ρ-coumaryl alcohol, which give rise to units of p'-hydroxyphenyl (H), guaiacyl (G) and syringyl (S) [24]. These subunits contain many different functional groups (e.g., hydroxyls (20–30%), carbonyls (20%) and methoxyls (90–95%)), which are active sites for further chemical modification of lignin [1, 25]. Lignin has key properties, such as biodegradability, thermal stability, reactivity, antioxidant and antimicrobial properties, an anti-inflammatory effect, biocompatibility, and low cytotoxicity [26, 27]. Based on these properties, lignin is biologically and mechanically suitable to be converted into advanced materials, including hydrogels, nanotubes, films, nanofibers, and nanoparticles, for various applications [6, 28–31].

Among these, hydrogels are characterized by a three dimensional (3D) network generated by the crosslinking of hydrophilic polymeric materials, which can have both natural and synthetic origins [32, 33]. Hydrogels exhibit viscoelastic or elastic behaviour and can be classified into two types: chemical or physical, depending on the nature

of the interactions that form the three dimensional (3D) network [1, 2]. Chemical hydrogels are those in which the network is formed through covalent bonds and this gives the final product different characteristics such as more resistant mechanical properties. Unlike chemical hydrogels, physical hydrogels are made up of weaker interactions generally hydrogen bonds, ionic forces, hydrophobic forces or van der Waals interactions. These kinds of materials have a variety of applications. In the field of cultural heritage conservation, several gel-based cleaning systems have been developed and optimized over the past decades, including agar and gellan gum rigid gels, as well as polyvinyl alcohol (PVA)-borax (B) hydrogels, which are among the most used [34–44]. PVA-borax (PVA-B) hydrogel is obtained by cross-linking of PVA with borate ions [34, 38, 45–47], which can be described as a viscoelastic dispersion with a dynamic network. In fact, the increase in borax concentration expands the system network due to electrostatic repulsions in the polymer chain [38, 46, 48]. The PVA-B systems have proven to be suitable for artworks cleaning thanks to their reversibility, ability to localize the treatment, ease of application, ease of removal by peeling, especially on vertical surfaces, and they do not cause secondary effects on the treated surfaces. Moreover, they can be loaded with active molecules that guarantee the selective removal of specific dirt, e.g., chelating agents, such as EDTA, can be incorporated to complex metal corrosion products [34, 43, 49]. Agar and gellan systems [39, 45, 50–54] are appreciated for their controlled water release and ease of removal, but their cleaning action is mainly based on solvent transport and limited mechanical interaction, without intrinsic chemical affinity toward specific metal ions. Conversely, PVA-borax systems loaded with chelators (e.g., EDTA) provide enhanced selectivity toward metal corrosion products through strong coordination mechanisms [35, 43, 49]. However, the use of synthetic chelating agents raises concerns related to their potential over-chelation, environmental persistence, and possible long-term effects on the substrate [43, 55]. In this context, the introduction of lignin into a PVA-borax network represents a conceptual shift: rather than incorporating an external synthetic chelator, the active functionality is provided by a bio-based macromolecule intrinsically rich in phenolic hydroxyl, methoxyl, and carboxyl-related groups. These functional moieties confer lignin a natural affinity toward metal ions through electrostatic interactions, hydrogen bonding, and possible coordination mechanisms. Therefore, the proposed lignin-based hydrogel combines the well-established rheological and mechanical advantages of PVA-borax systems with the metal-binding capability of a renewable biomacromolecule, potentially enabling a more sustainable and substrate-compatible alternative to conventional chelator-loaded gels.

Exploiting the properties of polyvinyl alcohol, borax and their combination, several lignin-based hydrogels have already been synthesized, both via chemical and physical crosslinking [1, 2, 56]. They are considered more sustainable and environmental-friendly compared to fully synthetic hydrogels and allow the reuse of waste lignin that is converted into a valuable by-product. Li et al. [57] reported that the couple PVA/lignin generates chemical networks after the previous modification by amination of sodium lignin sulfonate. Ciolacu et al. [58] mixed PVA with lignin or lignin-epoxy resins to produce hydrogels by covalent crosslinking with epichlorohydrin. Wu et al. [59] reported a simpler method based on PVA-lignin crosslinked with epichlorohydrin to obtain a doubly crosslinked network. Alternatively, physically crosslinked lignin-based hydrogels consist of the simple dispersion or blending of lignin into the 3D network and they have been mostly employed in the absorption of Cu(II) and Ni(II) metal ions for wastewater treatment. Among these, Huang et al. [60] proposed a formulation containing hydroxyethyl cellulose (HEC), PVA and borax with lignin physically crosslinked with the cited polymers. In this case, lignin acts as a plasticizer, increasing polymer chains' mobility, producing increased stretchability of the network. This system showed self-healing capability due to the dynamic hydrogen bonding and superabsorbent properties. Indeed, lignin polymer has phenolic hydroxyl groups and aromatic rings containing negatively charged oxygens [56]. These structures could strongly attract positive molecules and aromatic organics through negative functional groups and π-π reaction, respectively [61]. The absorption of inorganic ions usually refers to heavy metal ions, such as Cd (II), Pb (II), Ni (II), Cu (II), Co (II), and Hg (II) [62]. The capacity of absorption depends on the functional groups as well as the structure of hydrogels [56].

Thanks to their properties, the different lignin-based hydrogels could be considered as emerging materials with potential applications as drug delivery systems for agriculture or medicine, in water remediation applications, and in sensors since they can serve as absorbents for heavy metal ions, controlled release agent for controlled delivery and water retention, smart materials for stimuli response, and biosensors and electrodes [1, 29, 59, 60, 63]. In this scenario, a novel potential application of lignin-based hydrogels could be the cleaning of stone cultural heritage. Unlike traditional conservation gels, where metal selectivity is achieved by adding low-molecular-weight chelators, in the present system, lignin nanoparticles act as structurally integrated metal-binding domains within the hydrogel network. This approach aims to provide selective interaction with copper-based corrosion products while limiting excessive extraction of calcium ions from carbonate substrates, thus potentially improving compatibility with stone materials. To this end, this work aims at loading a PVA-B system, which represents one of the most tested gel-like material in the cleaning of artworks and whose rheological and mechanical properties

have been extensively studied in previous works [37–42, 44, 46, 48, 52], with lignin that can perform as an active molecule for the removal of metal ions from stone surfaces. Three different stones were artificially stained with metal corrosion products and then cleaned using the synthesized lignin-based hydrogel. Portable FTIR, single-sided NMR and colorimetry were used to assess non-invasively the performance of the hydrogel, and non-portable ATR-FTIR spectroscopy was used to characterize the hydrogel and understand the involvement of lignin in the cleaning mechanism.

Materials and Methods

Three carbonate stones with different porosity but similar chemical composition [40, 64–70] (mainly $CaCO_3$) belonging to three different lithotypes, Candoglia marble, Carrara marble and travertine, were used as test materials in this work. A total of four replicates for each lithotype was used. They were chosen because represent some of the most widespread stone materials in the Italian field of cultural heritage. The stone samples have a parallelepiped-like shape with a size of $5 \times 5 \times 2$ cm^3 and are displayed in Fig. 1.

A solution containing soluble metal salts obtained as previously shown by Giuliani et al. [35] from the reaction between two bronze disks (85% Cu, 5% Sn, 5% Pb, 5% Zn) and Copper (II) Sulphate ($CuSO_4$) was used along with several old euro cent coins made of copper-covered steel, to trigger the artificial deposition of the metal corrosion products on the three stone samples as described in Sect. "Artificial Staining of the Stone Samples".

For the lignin-based hydrogel synthesis the following reagents were used: polyvinyl alcohol (PVA) supplied by Sigma Aldrich (St. Louis, MO, USA) with Molecular weight (Mw) = 146,000 g/mol and hydrolyzation degree = 99%; di-Sodium tetra-Borate 10-hydrate (Borax, B), supplied by AppliChem (Germany); alkali lignin with Mw = 4300 g/mol and sodium hydroxide NaOH both supplied by Sigma Aldrich (St. Louis, MO, USA). Moreover, alkali lignin together with ethylene glycol and HCl purchased from Sigma Aldrich were used to synthesize the lignin-nanoparticles (LNPs) following the procedure used in Yang et al. [71].

Artificial Staining of the Stone Samples

The solution containing soluble metal salts was dripped on the stone surface using a pipette, then the aged euro coins were positioned on the surface. The reaction was allowed to proceed for two weeks, during which time further drops of metal salt solution were periodically added. After two weeks, the euro coins were removed and the stone surfaces appeared with differently colored stains, as shown in Fig. 2. Both greenish and brownish stains are visible, indicating the formation of corrosion products of different chemical nature. The powdered corrosion products were obtained by scraping the coins used to stain the samples and they were characterized using ATR-FTIR.

Lignin-Based Hydrogel Synthesis

Two different procedures were tested to load the PVA-borax hydrogel with lignin, as follows:

(1) In the first procedure, the powder of alkali lignin was used as it was without any modifications and 0.5 g of alkali lignin were dissolved in a solution of 0.4% of NaOH in distilled water. Then, a solution of 5 wt % of PVA in distilled water and a solution of 0.8% of borax in distilled water were prepared. To facilitate the PVA dissolution in water, the solution was magnetically stirred at 100 °C for 1 h. The PVA solution was then allowed to cool before adding the lignin solution under continuous stirring at room temperature. Finally,

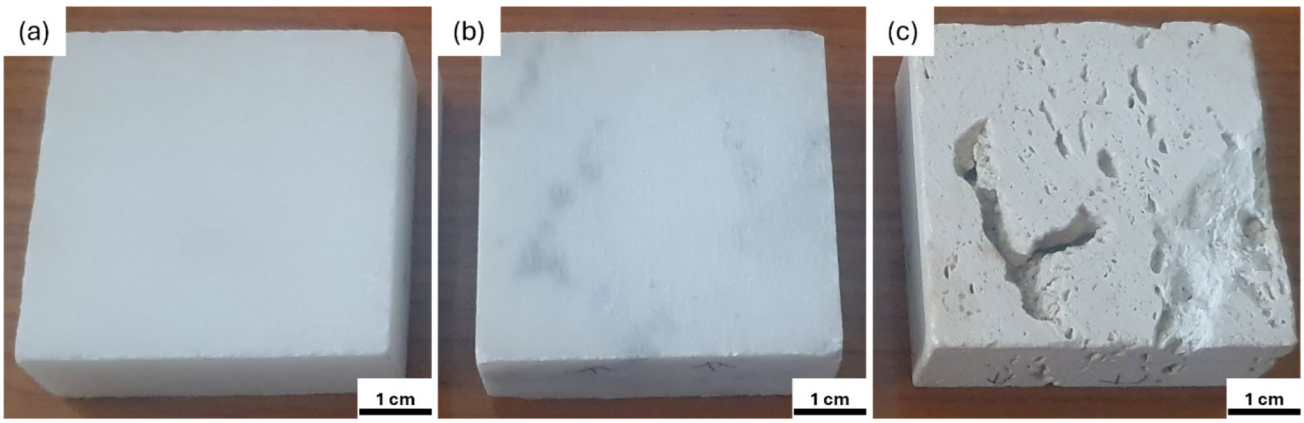

Fig. 1 **a** Candoglia marble, **b** Carrara marble and **c** travertine sample

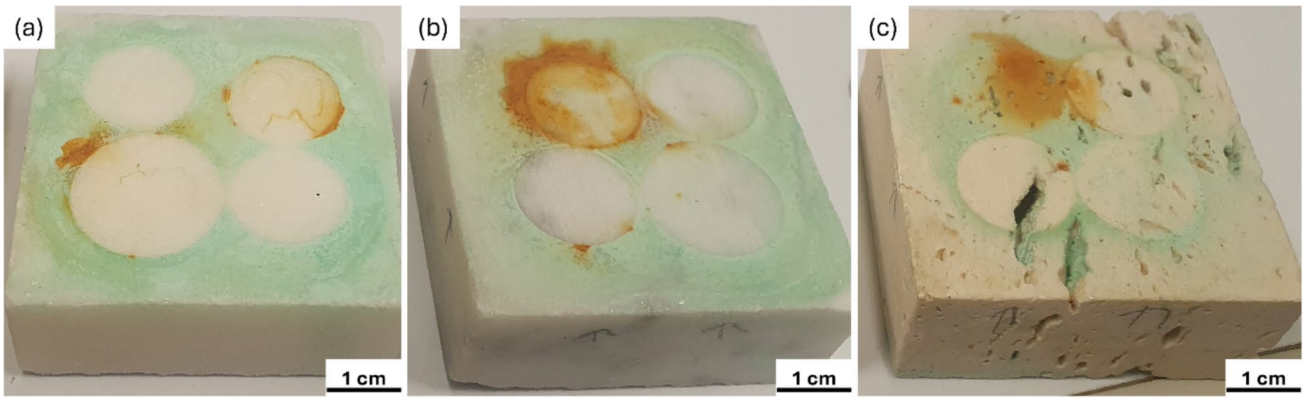

Fig. 2 **a** Candoglia marble, **b** Carrara marble and **c** travertine sample after the artificial staining with metal corrosion products

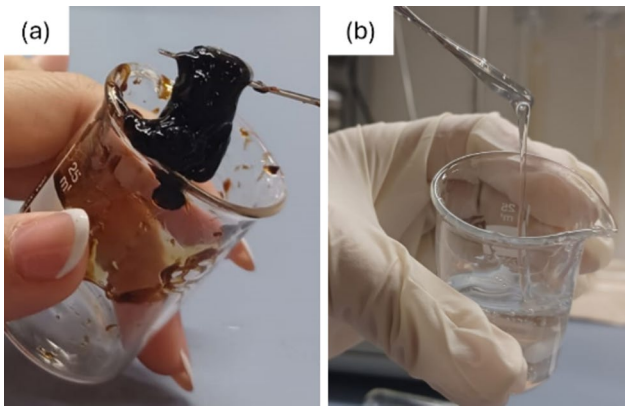

Fig. 3 PVA-borax hydrogel loaded with **a** alkali lignin and **b** lignin-nanoparticles (LNPs)

a total of 450 µl of borax solution were dripped into the PVA-lignin solution until gelation occurred. The result is an elastic dark brown hydrogel displayed in Fig. 3a.

(2) In the second procedure, instead, the alkali lignin was first converted into lignin-nanoparticles (LNPs) by hydrochloric acidolysis as described in Yang et al. [71], with some modifications. Briefly, a 4% solution of lignin in ethylene glycol was prepared and stirred at 35 °C for 1 h. After, the pH of the solution was adjusted to 2.5 by adding 3 drop/min of HCl 0.25 M and retained for 2 h. The solution was then filtrated with 0.45 µm cellulose acetate syringe filters to remove insoluble impurities and dialyzed against deionized water for 3 days obtaining a final pH = 7. This dialysis step removes the majority of the ethylene glycol from the suspension. Consequently, the final hydrogel formulation used during the cleaning tests contains lignin nanoparticles dispersed mainly in water, with only negligible residual traces of ethylene glycol. The suspension was transferred into a flacon and sonicated for 30 min. Finally, two different centrifugation steps have been carried out, at 1.47 rcf to precipitate the NPs bigger than 250 nm and collecting those ≤ 250 nm which remain in the supernatant. The centrifugation time was optimized by evaluating the hydrodynamic diameter (D_H) through Dynamic Light Scattering (DLS) measurements (Supplementary Information). The morphology and stability of LNPs were evaluated by scanning electron microscopy (SEM) and zeta potential (ζ) measurements respectively (Supplementary Information). After filtration and centrifugation, a rather homogeneous suspension of 10 wt% of LNPs (with mean size around 50 nm) in water and ethylene glycol was obtained. Subsequently, a solution of 4 wt% of PVA in distilled water and a solution of 0.8% of borax in distilled water were prepared. To facilitate the PVA dissolution in water, the solution was magnetically stirred at 100 °C for 1 h. The PVA solution was then allowed to cool and a total of 2 ml of LNPs suspension was added under continuous stirring at room temperature. Finally, a total of 350 µl of borax solution was dripped into the PVA-LNPs solution until gelation occurred. The result is a quite elastic and transparent hydrogel displayed in Fig. 3b. The pH of the hydrogel was measured prior to its application on the stone surfaces. The measured pH of the final PVA–borax–LNPs hydrogel was approximately neutral.

Additionally, two different formulations made of PVA-borax and PVA-LNPs, respectively, were prepared as follows: 400 ul of borax solution (0.8%) was added to 10 ml of solution of PVA (4 wt%); 2 ml of LNPs suspension were dispersed into 10 ml of PVA (4 wt%). The PVA-borax and PVA-LNPs formulations were used during preliminary cleaning tests (described in Supplementary Information) for comparison with the results obtained using the

PVA-borax-LNPs hydrogel and to understand the involvement of lignin in the metal ions sequestration.

Cleaning Tests

The dark brown colour of the hydrogel containing alkali lignin immediately appeared unsuitable for cleaning white stone surfaces. However, it was tested anyway and applied in a small portion on the surface of an untreated Candoglia marble sample (Fig. 4a). After a few minutes, a dark spot appeared on the surface of the stone (Fig. 4b), so the hydrogel was quickly removed to avoid further staining. In conclusion, this hydrogel turned out to be unsuitable for cleaning stones because even from a macroscopic point of view, the gel appears to stain the surface, thus providing a side effect and irreversible treatment.

The transparent hydrogel obtained from the incorporation of LNPs into the PVA-B system was used to clean the artificial stained stones. A thin layer of the LNPs-PVA-B hydrogel was applied for 4 h on one half of the surface of Candoglia marble, Carrara marble, and Travertine, as shown in Fig. 5. Cleaning tests were replicated on the four different samples for each lithotype. During the cleaning tests, the hydrogel was applied at a loading of 0.16 g/cm^2.

Then, the hydrogel layer was peeled off with the help of a spatula, and the application was repeated again for the same time. After the two application steps of 4 h each, which were required to ensure sufficient drying of the hydrogel and facilitate the peeling procedure, according to previous studies [35, 40, 72], the half of the stones surface appeared not homogeneously cleaned, as shown in Fig. 6.

Portable FTIR Measurements

A Bruker Alpha II instrument was used to acquire FTIR spectra directly on the surface of the stones before and after the artificial staining and after cleaning using the LNPs-hydrogel. The instrument allows external reflectance FTIR (ER-FTIR) measurements in a non-invasive way from a surface area of about 1.0 × 2.0 cm^2 of the sample. The OPUS software was used to set the experiments. The spectra were collected in the range 4000–400 cm^{-1}, with a resolution of 2 cm^{-1} and 40 scans were accumulated for each spectrum. The background was acquired on the air with a gold flat mirror before each analysis. Since ER-FTIR is influenced by surface roughness and porosity, especially in heterogeneous substrates such as travertine, measurements were performed maintaining a consistent acquisition geometry (probe–surface distance and angle) for all samples, to minimize these effects. Moreover, spectra were collected on representative areas of the samples, and three measurements were performed at different points of each stone surface. The resulting spectra were then compared to assess reproducibility and averaged to obtain a representative signal. In addition,

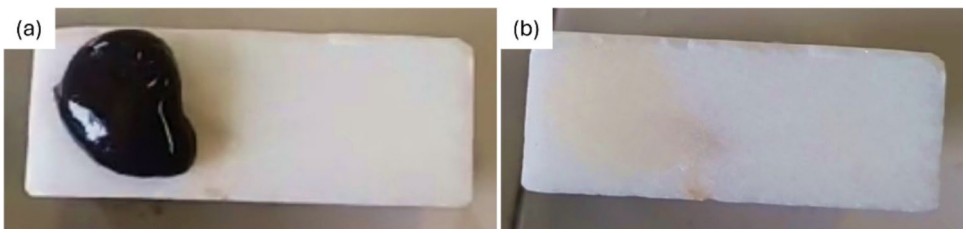

Fig. 4 Candoglia marble surface **a** during the application of the hydrogel containing alkali lignin and **b** after its removal with the visible brown stain left by the gel

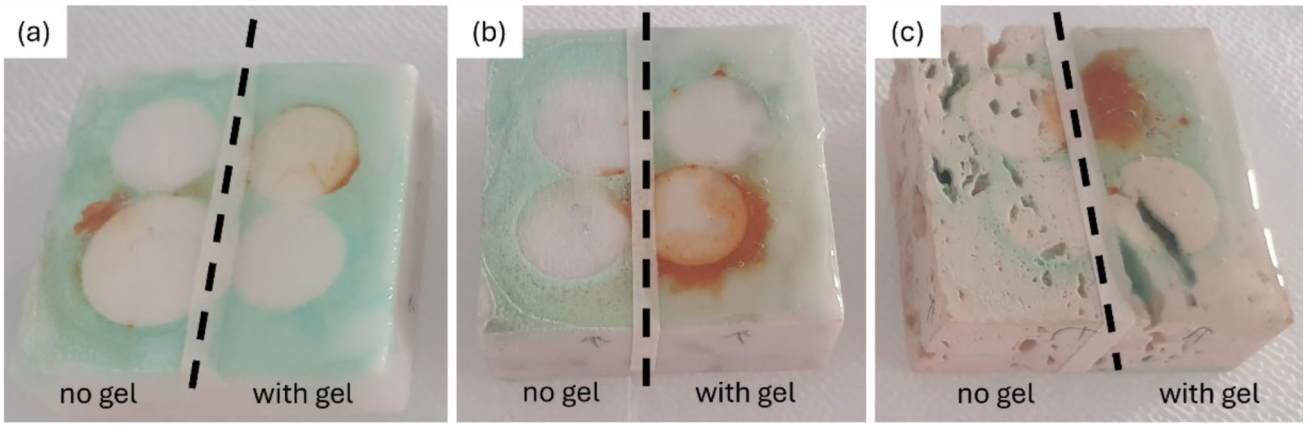

Fig. 5 Thin layer of the hydrogel loaded with LNPs applied on one half of the stained surface of **a** Candoglia marble, **b** Carrara marble and **c** Travertine

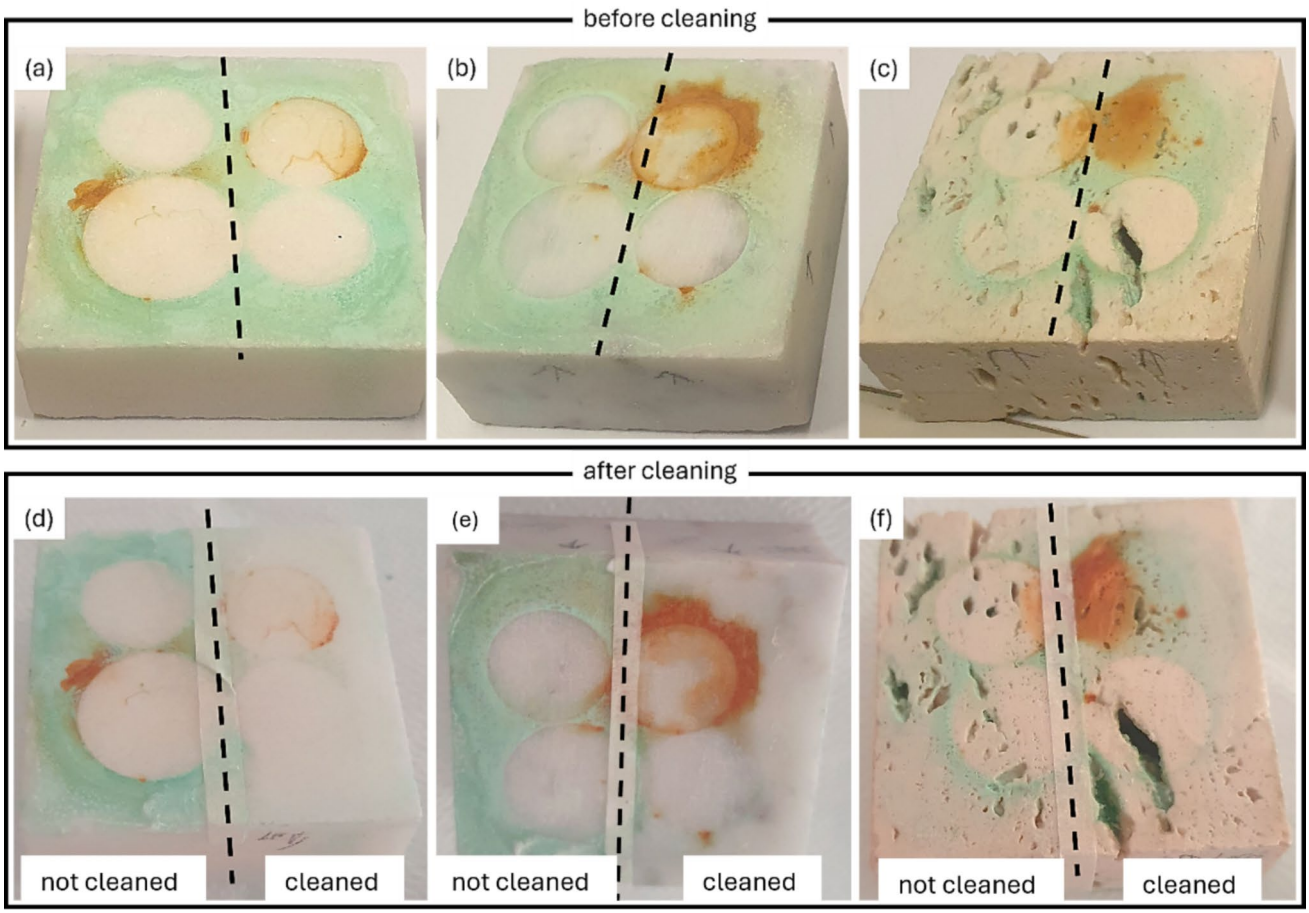

Fig. 6 Half of the surface of **a**, **d** Candoglia marble, **b**, **e** Carrara marble and **c**, **f** travertine before and after being cleaned with the hydrogel loaded with LNPs

all spectra were processed using normalization to reduce variability due to differences in reflectance intensity. Furthermore, Kramers–Kronig Transformations (KKT) were applied in the whole range by using the related OPUS tool. The data processing was carried out using MATLAB 2024 and Origin 9.0 software (©OriginLab, USA). In order to compare the cleaning performances of the three different formulations, ER-FTIR spectra (see Supplementary Information) were acquired on three different areas of each lithotype before the cleaning and after the cleaning with three different formulations: PVA-borax (PVA-B), PVA-LNPs and PVA-borax-LNPs (PVA-B-LNPs). The three measurements, after assessment of reproducibility and averaged, were subjected to KKT. The following Recovery Index (RI) was calculated:

$$RI = \frac{\nu_{stain} - \nu_{clean}}{\nu_{stain} - \nu_{ref}} \quad (1)$$

where ν_{stain} is the frequency of carbonate stretching peak maximum (range: 1400–1580 cm^{-1}) for the stained stone, ν_{clean} is the frequency of this peak after the cleaning, and ν_{ref} is the frequency of the same peak in the unstained material. RI varies between 0 (no recovery of the original frequency) and 1 (total recovery of the original frequency). The higher the value of the index, the higher the recovery of original frequency of carbonate stretching peak: this could be considered representative of cleaning performances towards the corrosion products, whose removal would allow the appearance of the original signals of the stone material. From this point of view, it is fundamental to highlight that the Recovery Index may not be representative of all the degradation phenomena—it does not take into account of possible distortion or broadening of the signals, and it does not provide any hint about the chromatic variation—but it is selected because of its relation to chemical signals attributable to the unstained materials, so it represents an accessible parameter to monitor the performances of the gel formulations.

Portable NMR Measurements

Portable NMR was used to monitor the contamination process and to assess the cleaning efficacy of the hydrogel loaded with LNPs in removing metal corrosion products from the three carbonate stone surfaces. Specifically, NMR measurements were performed, in a non-invasive way, using an NMR-MOUSE portable spectrometer equipped with an open magnet that generates a magnetic field of 0.35 T and a radiofrequency probe that receives the NMR signal coming from 2 mm deep below the sample surface. Candoglia marble, Carrara marble, and travertine samples, along with the portable NMR probe, were placed in an insulating box to keep the relative humidity (RH) and temperature (T) under control, avoiding oscillations. Specifically, the RH and T correspond to those present in the laboratory room and were respectively RH = (50.0 ± 3.5)% and T = (24.0 ± 1.0) °C. The microclimatic conditions in the insulating box were monitored with a TROTEC® BC06 thermo-hygrometer. The spin–spin relaxation time T_2, which is sensitive to water proton mobility and to the magnetic field inhomogeneities induced by paramagnetic ions, was quantified with a Carr-Purcell Meiboom-Gill (CPMG) sequence [73] on the entire half surface (corresponding to the probe sensitive area of about 5.0 × 1.5 cm^2) of the untreated and stained samples and on those cleaned with the hydrogel. The CPMG sequence was characterized by a number of scans (NS) = 2048, repetition time (TR) = 0.5 s, number of echoes = 500, echo time (TE) = 0.03 s, and acquisition time (AT) = 25 min. Each measurement was repeated three times to assess reproducibility and an average signal was obtained. The Minispec® software was used to run and control the NMR experiments. The T_2 distributions were reconstructed in MATLAB 2024 using the Inverse Laplace Transform (ILT) method [74–77]. Moreover, a semi-quantitative analysis was performed based on the calculation of the weighted average T_2 and on the variations in peak intensity. A recovery index based on the weighted average T_2 was also calculated as:

$$RI_{T2} = 1 - \frac{\left|T_{2cleaned} - T_{2untreated}\right|}{\left|T_{2stained} - T_{2untreated}\right|} \quad (2)$$

where $T_{2untreated}$, $T_{2stained}$, and $T_{2cleaned}$ are the weighted mean T_2 values measured on the untreated, stained, and cleaned stone surfaces, respectively. An RI_{T2} value equal to 1 indicates complete recovery of the untreated condition, whereas 0 indicates no recovery. Negative values indicate that the cleaned surface remains farther from the untreated condition than the stained one, likely due to the combined effect of residual corrosion products, modified water mobility, and possible hydrogel residues.

Colorimetric Analyses

For the colorimetric measurements, a Visible Light spectrometer BW&Tek Exemplar LS, equipped with a fibre optic, a 45° degree holder and a Tungsten lamp, was used. For every spectrum, 5 scans were accumulated, with an acquisition time of 500 ms. The colorimetric data (L*, a* and b* coordinates) were calculated from the reflectance through the acquisition software, BWSpec, with reference to a D65 illuminant (10° Observer). Colorimetric data were acquired in two different areas from the stone materials, before and after the cleaning. For the estimation of cleaning performances, ΔE was calculated with reference to the colorimetric coordinates of an unstained area of the stones, representative of the optical properties of the different lithotypes.

ATR-FTIR Measurements

FTIR spectra in Attenuated Total Reflection (ATR) mode were acquired using a Nicolet iS50 FTIR spectrometer combined with a built-in ATR system and elaborated by the OMNIC software©. The dry layers of PVA-B-LNPs hydrogel used to clean the stone surfaces, shown in Fig. 5, were placed onto the diamond cell and the spectra were collected from different points. Moreover, the ATR-FTIR spectra of the dry gel-like layers of PVA-borax and PVA-LNPs formulations were acquired before and after being used to clean the stones (see Supplementary Information) and were compared with those acquired on the PVA-borax-LNPs formulation. The powder of corrosion products scraped from the coins were also characterized using ATR-FTIR. The spectral range was 4000–400 cm^{-1}, with a resolution of 4 cm^{-1} and 32 scans were accumulated for each spectrum. The background was acquired on the air before each analysis, and a minimum of three analyses

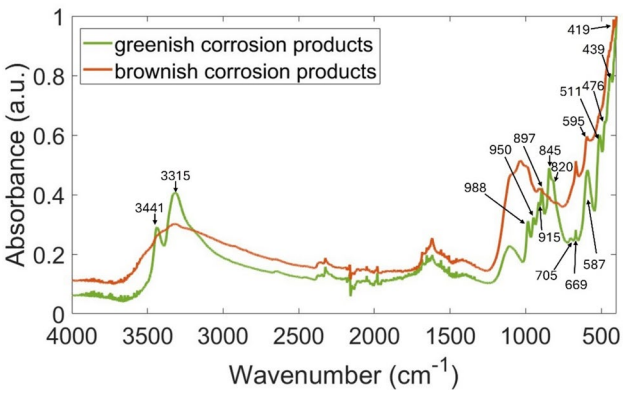

Fig. 7 ATR-FTIR spectra of the corrosion products scraped from the coins used to stain the stone samples

were performed for each specimen. Finally, the data processing was carried out using Origin 9 and MATLAB 2024. A semi-quantitative analysis was performed calculating the variations of ATR-FTIR peaks' intensity ratios.

Results and Discussion

In this work, portable ER-FTIR and NMR were used to analyse the stone surfaces before and after their artificial contamination with metal corrosion products, and after the application of the lignin-based hydrogel to remove these corrosion products. Along with these techniques, colorimetry was used to support the evaluation of the cleaning efficacy of the PVA-B-LNPs hydrogel. The hydrogel layers were then peeled off from the stone surface and left to dry in order to be analysed by ATR-FTIR and compared with the PVA-B and PVA-LNPs formulations to understand if metal ions were entrapped by lignin. Moreover, the corrosion products were characterized by ATR-FTIR directly on the powder scraped from the metal coins. In the following sections the results obtained from portable ER-FTIR, NMR and colorimetry and those from non-portable ATR-FTIR are discussed.

ATR-FTIR Characterization of the Corrosion Products

Concerning the green product of the patina scraped from the coins, the FTIR-ATR spectra in Figure 7 show bands at ~ 3441 cm^{-1} and ~ 3315 cm^{-1} attributable to O–H stretching vibration of the hydroxyl group [78, 79]. The absorption pattern observed in the region 1700–1300 cm^{-1} are related to O–H-O bending modes [80]. Bands at ~ 988 cm^{-1}, ~ 950 cm^{-1}, ~ 915 cm^{-1}, ~ 897 cm^{-1}, ~ 845 cm^{-1} and ~ 820 cm^{-1} are likewise assigned to O–H bending (deformation) vibrations of the same hydroxyl groups [78, 79]. The peaks at ~ 587 cm^{-1}, ~ 511 cm^{-1}, ~ 476 cm^{-1} and ~ 439 cm^{-1} can be correlated to the stretching of the Cu–O and Cu–Cl bonds, typical of atacamite [78]. The split peak at ~ 1108 cm^{-1} and ~ 1073 cm^{-1} can be related to the SO_4 asymmetric stretching [81], whereas the peaks at ~ 705 cm^{-1} and ~ 669 cm^{-1} are assigned to the S–O ν_4 bending vibration [82–85], indicating the presence of sulphates. In the case of brown patina, the ATR-FTIR spectrum shows a broad band at ~ 3320 cm^{-1}, related to O–H stretching vibrations. Additionally, the ~ 1617 cm^{-1} peak corresponds to O–H–O bending modes. Peaks between ~ 1107 cm^{-1} and ~ 989 cm^{-1} can be related to the symmetric and asymmetric stretching of SO_4 [81], whereas the peak at ~ 668 cm^{-1} can be assigned to the S–O ν_4 bending vibration [82–85], confirming the presence of sulphates. As in the previous spectra, the broad peak at ~ 915 can be assigned to O–H bending vibrations, whereas ~ 595 cm^{-1} and ~ 419 cm^{-1} can be associated with the stretching of the Cu–O and Cu–Cl bonds in copper chloride compounds.

Portable ER-FTIR and NMR Monitoring of the Stone Surfaces

Figure 8 shows the external reflectance FTIR spectra of the stone surfaces of Candoglia marble, Carrara marble, and travertine before and after their contamination.

The ER-FTIR spectra acquired on the untreated stones show all the characteristic peaks of calcite, as it represents the main constituent of the three lithotypes. After the contamination process, a series of signals could be observed, which could be considered indicative of the formation of copper corrosion products of different typology and with a certain variability all over the surfaces of the stones. In the low wavenumber region (indicated by the dotted line rectangle), variable signals could be observed, with two main ones around 488 and 530 cm^{-1}, which would be consistent with bands characteristic of copper sulphates, such as brochantite ($Cu_4(SO_4)(OH)_6$)) [86]. The increase of pseudo-absorbance signals at 852 (overlapping with the reststrahlen band at 875 cm^{-1} of calcite), 921, 954, and 990 cm^{-1} could

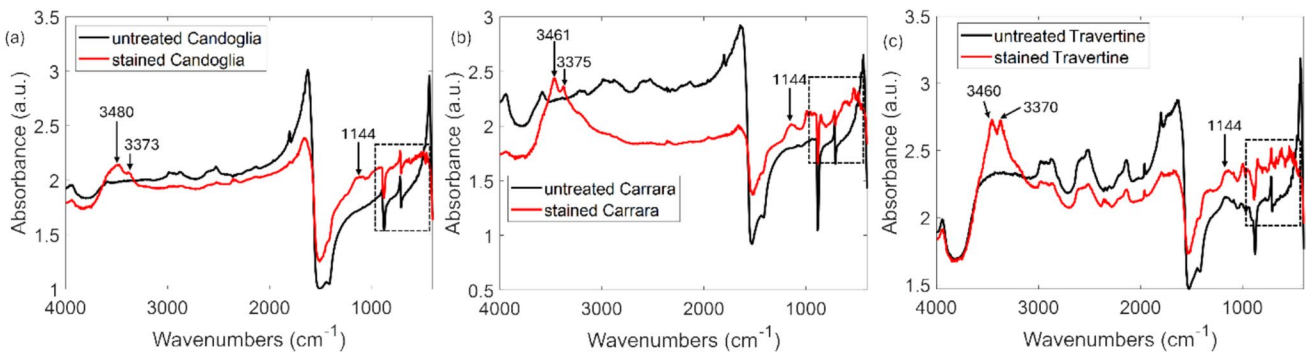

Fig. 8 ER-FTIR spectra of **a** Candoglia marble, **b** Carrara marble and **c** travertine before (black line) and after (red line) artificial contamination with metal corrosion products

be attributed to chlorinated copper compounds, such as atacamite ($Cu_2Cl(OH)_3$) and paratacamite ($(Cu,Zn)_2(OH)_3Cl$) [87]. The presence of chloride could be ascribed to the previous ageing process of the eurocent coins. In some areas of the three stones, an increase of pseudo-absorbance with a broad band at around 1144 cm^{-1} could be assigned to the stretching of the SO_4^{2-} group and it would confirm the presence of copper sulfates with different hydration degrees [86]. The increase of two strong peaks between 3480 and 3370 cm^{-1} could be related to variation in the OH stretching ascribable to the formation of corrosion products with different hydration degrees: in particular, according to the literature, these signals would be attributable to atacamite and paratacamite [87]. All these attributions are supported by the ATR findings. Finally, some variations are also observable in the carbonate region between 1350 and 1600 cm^{-1}, but the strong interference of calcite reststrahlen band with minima at 1410 and 1520 cm^{-1} does not allow further observations. However, the composition of the corrosion stains is probably more complex, as also proofed by some Raman spectra (Supplementary Information, Fig. 2S): the bands at 150 and 215 cm^{-1}, observable in some spectra acquired in correspondence of brownish stains, are attributable to cuprite Cu_2O, while a series of broad bands between 430 and 760 cm^{-1} would be likely indicative of defective Cu_2O and hydroxyl-salts of Cu(II). The bands around 275 and 395 cm^{-1} are not easily attributable with reference to the literature, even if they could show some similarities with the pattern of tenorite CuO. Another possible hypothesis could rely on the association of the two strong bands at 215 and 275 cm^{-1}, which could be even indicative of iron sulphates, probably deriving from metal coin core [88]. Finally, a low intensity band at 983 cm^{-1} could confirm the presence of either antlerite or brochantite [89–93]. Even if uncertainty in the Raman assignations must be taken into account, signals not directly attributable to the species individuated by FTIR support the chemical complexity of the corrosion products, also with reference to the different resolution of the technique. After the application of the lignin-based hydrogel, the ER-FTIR spectra shown in Fig. 9 were collected from two different regions of the cleaned surface of each stone sample. This choice was necessary because of the inhomogeneous cleaning action visible to the naked eye. Anyhow, the hydrogel seems more effective in the removal of the greenish stains rather than the brownish stains.

In the Candoglia marble, region 1 corresponds to a better cleaned area, as confirmed by the ER-FTIR spectrum, which shows the disappearance of the OH bands at 3480 and 3370 cm^{-1} and a general decrease of the pseudo-absorbance intensities of corrosion products in the low wavenumber regions. Conversely, region 2 still presents a stain, and the respective ER-FTIR spectrum is still affected by the presence of corrosion products, as indicated by the same OH bands, which are less evident but visible. In Carrara marble, the spectrum of region 2 suggests the removal of almost all metals contributions, and all characteristic peaks of calcite are better visible. In contrast, in region 1, there is still a contribution from corrosion products in peaks at 488, 530, 3461 and 3375 cm^{-1}, while the features between 900–1000 cm^{-1} and the band around 1144 cm^{-1} are less evident. In the case of travertine, the weak variation in the FTIR spectra before and after cleaning in both regions indicates that the corrosion products are still present on the entire sample surface.

To provide a clearer correspondence between the visual data and the FTIR spectra and with reference to the typical deformations due to the reflection mode, KKT were applied (Fig. 10), which resulted particularly useful to investigate the range of CO_3^{2-} stretching. From the comparison of the KKT spectra for every stone, it is possible to classify the cleaning action of the gel on the different lithotypes, rather than improving phase identification. It is clear for all the stones that the staining corresponds to a general broadening of the spectrum, especially at higher wavenumbers, and a shift of the carbonate stretching pattern towards higher wavenumbers. These phenomena are likely attributable to the formation of hydrated compounds, which have combination and overtone bands of OH groups in the 1600–1800 cm^{-1} region [87]. After the cleaning, for Candoglia marble, it is possible to observe that the spectra in the investigated areas match the original spectrum, with only a slight broadening around 1580 cm^{-1} for region 2, while the maximum of the band is recovered. About Carrara marble, region 1 and region 2 would show different cleaning performances, as assessed by visual inspection and preliminary analysis of unprocessed reflectance spectra: for region 2, the carbonate signals present a spectral pattern similar to the original features, from both the point of view of the broadening and the maximum, while for region 1 this is intermediate between the untreated and the stained sample. Finally, for travertine, the spectra show a recovery of the maximum value of the band in both the testes, with a less but still evident broadening of signals, especially in region 2. This variability would be consistent with the different surface and porosity properties of the three lithotypes, and it is amplified by the chemical complexity of the corrosion products. With reference to this aspect, to achieve a semi-quantitative evaluation of the cleaning performances of the gel and to compare the effect of its different components, the frequency shift in KKT spectra was used. For this reason, three different formulations were tested for the cleaning: PVA-borax (PVA-B), PVA-LNPs, PVA-B-LNPs. The difference in frequencies of the maximum of the carbonate stretching peak before and after the cleaning with reference to the same peak in the unstained lithotype was calculated for all the formulations to evaluate the Recovery Index (Table 1). In all the cases, it is possible to observe that the cleaning with the formulations corresponded to a partial

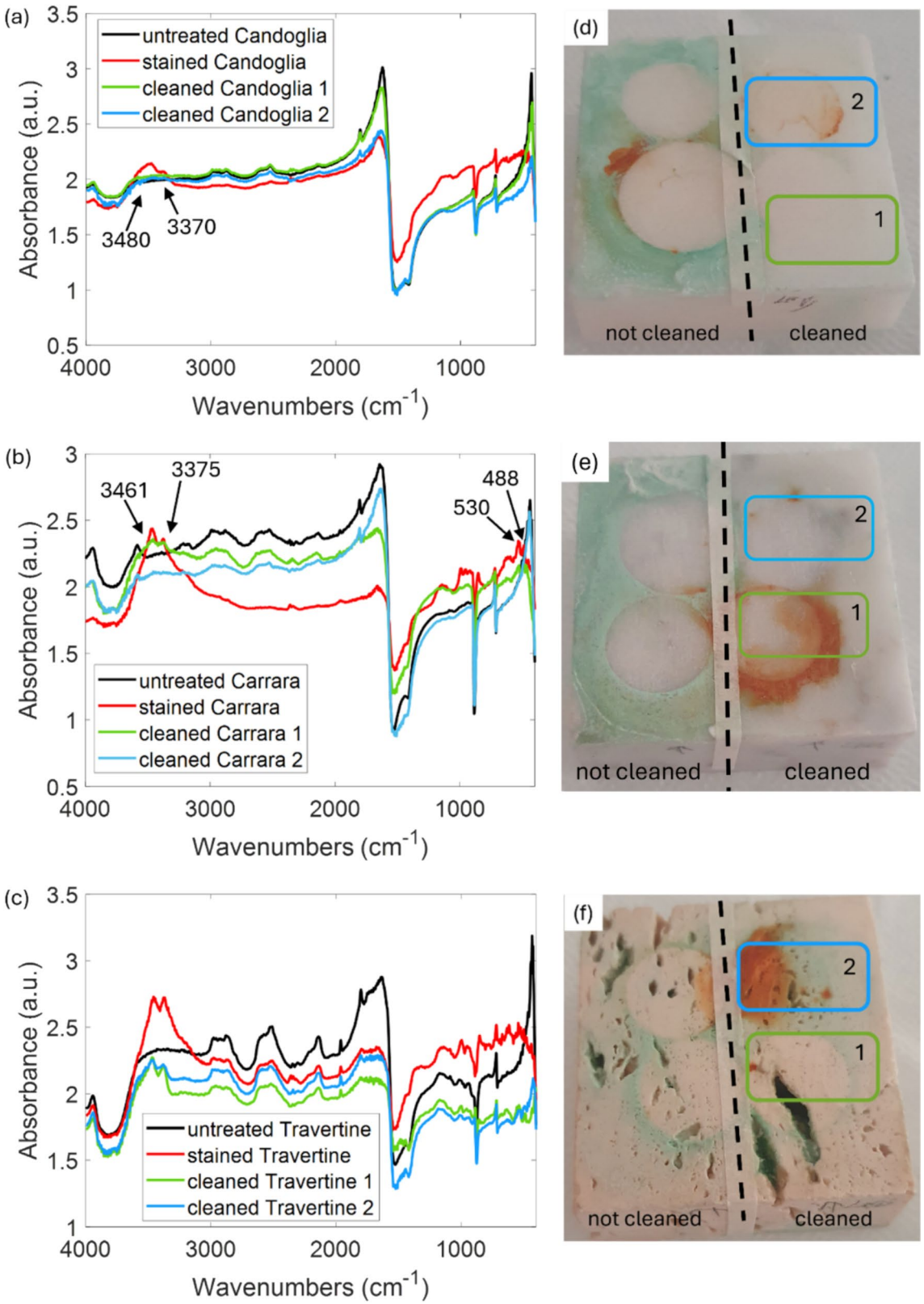

Fig. 9 ER-FTIR spectra collected from region 1 (green) and region 2 (light blue) on the hydrogel-cleaned surface compared with the ER-FTIR spectrum of stained (red) and untreated (black) surface of Candoglia marble **a**, **d**, Carrara marble **b**, **e** and travertine **c**, **f**

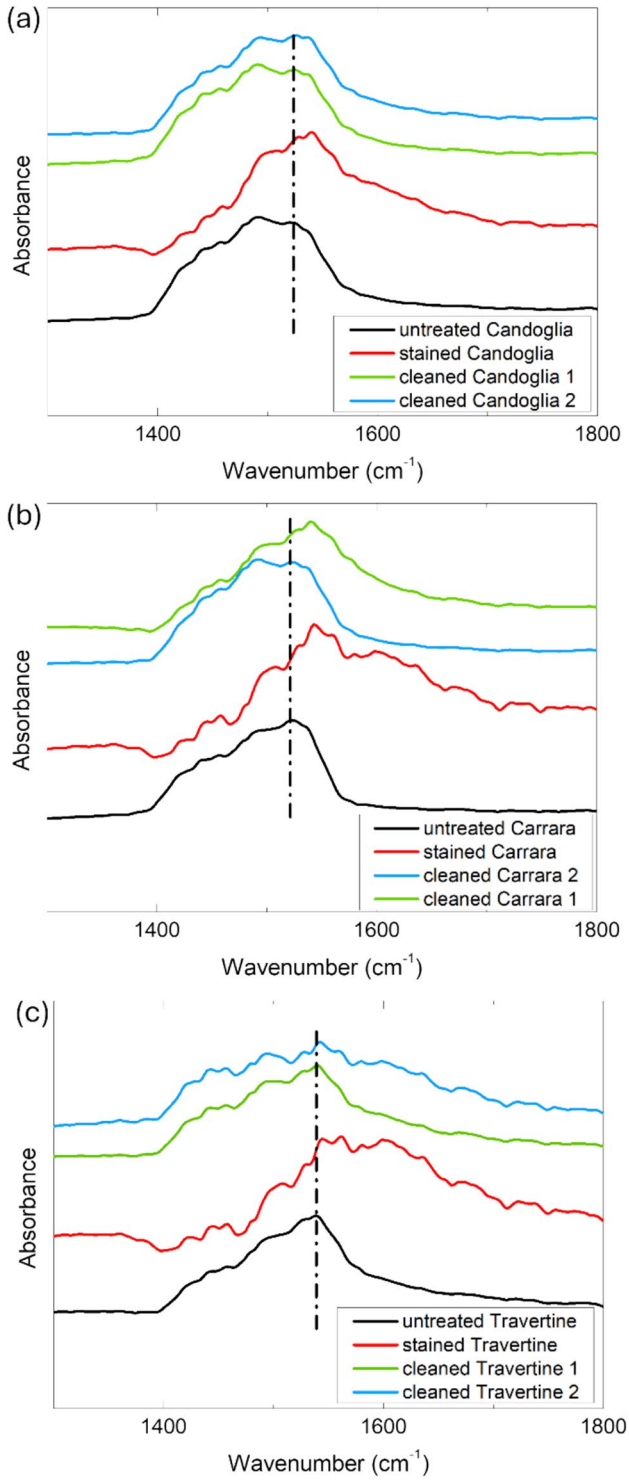

Fig. 10 KKT of the ER-FTIR spectra in the range of CO_3^{2-} stretching for the untreated (black line), stained (red line) and cleaned with LNPs-gel (green and light blue lines) surface of **a** Candoglia marble, **b** Carrara marble and **c** travertine

Table 1 Values of Recovery Index calculated using Eq. (1) for the tested formulations applied to the different lithotypes

Formulation	Recovery index		
	Candoglia	Carrara	Travertine
PVA-B	0.20	0.19	0.44
PVA-LNPs	0.14	0.03	0.53
PVA-B-LNPs	0.27	0.26	0.67

recovery of the frequency value, which is indicative of the efficacy of the cleaning. Moreover, for all the lithotypes, the PVA-B-LNPs formulation resulted in a higher recovery, proving a combination effect of borax and LNPs, which suggests the cleaning efficiency of this formulation is higher in comparison to its analogues. Finally, the Recovery Index would suggest that the best performances were obtained in the case of travertine, while for Carrara and Candoglia marbles the performances could be considered generally similar. This apparent contradiction with the optical data could be explained based on the whole ER-FTIR spectra and the porosity of the travertine in comparison to the marbles. In travertine, the higher porosity of the stone could have involved a higher penetration of corrosion products, with consequent higher difficulties in a complete removal (in the ER-FTIR spectra, signals of corrosion products are clearly evident after cleaning, as long from visual observation). However, on the surface exposed to the contact with the gel, the removal could have been highly effective, with a higher efficiency of the cleaning (re-appearance of the original carbonate peak) in comparison to the grade of the staining, as suggested by the Recovery Index.

With reference to these hypotheses, NMR analyses could provide further information. The T_2 distributions obtained by portable NMR are displayed in Fig. 11. It is worth noting that while for the FTIR acquisitions it was possible to collect spectra from two different regions of the stone surface to assess the heterogenous cleaning operated by the gel, for the NMR experiments it was only possible to analyse the entire zone of the stone surface treated with the gel, due to the size of the sensitive area of the NMR probe that has roughly the same dimension of the stone portion on which the gel was tested. This means that the spin–spin relaxation time T_2 measured is a mean value over the differently cleaned zones of the stone, providing further information on the overall performance of the gel. The T_2 parameter is sensitive to hydrogen mobility and to the presence of paramagnetic ions (such as copper and iron ions). Therefore, T_2 provides information on the stone surface variations during the staining process and its value after cleaning should return to the original value measured on the untreated stone. Moreover, T_2 can be used not only to evaluate the removal of metal ions from stone surface but also to measure changes

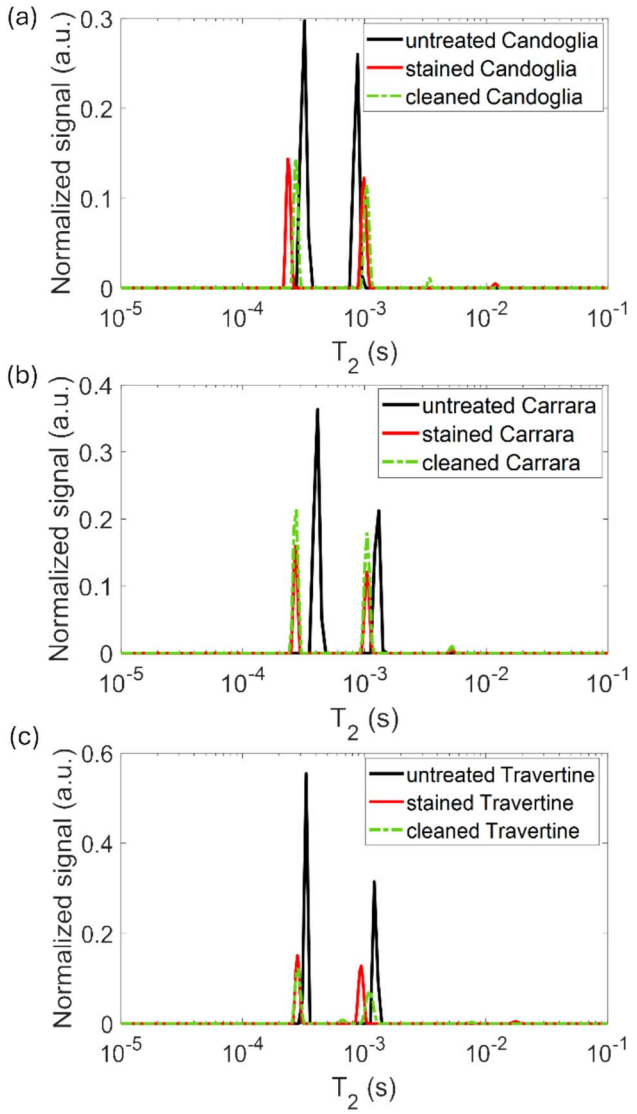

Fig. 11 T_2 distribution of the untreated, stained and cleaned surface of **a** Candoglia marble, **b** Carrara marble and **c** travertine

in water mobility and understand gel-substrate interaction, detecting the presence of gel residues. All untreated samples are characterized by two T_2 components: one around 0.3–0.4 ms and one around 0.9–1.3 ms. These two T_2 populations identify two different hydrogen populations: one more mobile (larger pores), associated with the longer T_2, and one less mobile (smaller pores), associated with the shorter T_2. After the artificial contamination, both the T_2 components decrease for Carrara marble and travertine, whereas in Candoglia marble the longest T_2 increase. This result suggests the shortening effect of paramagnetic corrosion products on the spin–spin relaxation time. Specifically, the shortening effect was stronger in Carrara marble where the brownish stain was bigger (Fig. 6b). This indicates that the brownish spot is composed of metal ions (iron, copper) that more strongly influence spin–spin relaxation. Furthermore, the increase of the T_2 around 1 ms in Candoglia marble can be ascribed to the formation of highly hydrated corrosion products with relatively mobile hydrogen environments. After the cleaning process using the lignin-based hydrogel, in all samples the T_2 distributions partially shift toward the values measured in untreated samples, indicating partial removal of paramagnetic species. However, the relaxation times do not fully return to their original values, suggesting that corrosion products remain on the surface and that a minor contribution from hydrogel residues may still affect the hydrogen mobility. Specifically, in the case of Candoglia marble and travertine, respectively, the shortest T_2 and the longest T_2 component became closer to those measured on the untreated surface. This result agrees with the ER-FTIR results. In the case of Carrara marble, where the brownish stain was considerably bigger than those present on Candoglia and travertine samples, the T_2 value, which is a mean over the entire surface, suggests that on average the stone surface was not cleaned by the gel as testified by the incipient brownish stain visible to the naked eye even after cleaning (Fig. 6e).

The semi-quantitative analysis of peak intensities (Tables 2 and 3) confirms these trends. Travertine shows the largest variation, with a significant increase in the intensity of the $T_{2,1}$ component (+9%) and a decrease of the $T_{2,2}$ component (−9%), suggesting a redistribution of hydrogen populations with different mobility. Conversely, Candoglia and Carrara marble show smaller intensity variations, indicating a less pronounced modification of the pore water environment after cleaning.

The weighted mean T_2 and its variation (Δ) are reported in Table 4 and further support this interpretation. The

Table 2 Peak intensity (%) associated with the $T_{2,1}$ component and its variation (Δ) after cleaning

Lithotype	Untreated (%)	Stained (%)	Cleaned (%)	Δ Cleaning versus stained (%)
Candoglia	58	54	56	2
Carrara	58	57	54	−3
Travertine	56	54	63	9

Table 3 Peak intensity (%) associated with the $T_{2,2}$ component and its variation (Δ) after cleaning

Lithotype	Untreated (%)	Stained (%)	Cleaned (%)	Δ Cleaning versus stained (%)
Candoglia	42	46	44	−2
Carrara	42	43	46	3
Travertine	44	46	37	−9

Table 4 Weighted mean of T_2 in ms with associated errors (±) and its variation (Δ) in % calculated after staining and after cleaning of stone surface, along with the recovery index (RI_{T2}) calculated from Eq. (2)

Lithotype	Untreated (ms)	Stained (ms)	Cleaned (ms)	Δ Staining (%)	Δ Cleaning (%)	RI_{T2}
Candoglia	0.389 ± 0.027	0.583 ± 0.027	0.615 ± 0.014	49.90	5.50	− 0.165
Carrara	0.545 ± 0.030	0.606 ± 0.025	0.628 ± 0.016	11.20	3.60	− 0.361
Travertine	0.579 ± 0.018	0.586 ± 0.026	0.589 ± 0.036	1.20	0.50	− 0.429

strongest variation for Candoglia marble, where the average relaxation time increases by nearly 50% after staining, indicates the formation of highly hydrated corrosion products that strongly affect the T_2 of the surface. After cleaning, the weighted mean T_2 increases only slightly (+ 5.5%), suggesting partial removal of corrosion products together with possible residual hydrogel contribution. In contrast, the weaker variation observed in Carrara marble and travertine suggests a more limited modification of the hydrogen environment after staining. Particularly, in the case of travertine, the lower variation in the mean T_2 after staining is observed and this may suggest that the corrosion products migrate deeper in the porosity of travertine compared to Candoglia and Carrara marble rather than remaining confined on the surface. The RI_{T2} calculated from Eq. (2) using the weighted mean T_2 gave negative values for all samples, indicating that the cleaned surfaces did not return to the untreated condition. This suggests that the weighted mean T_2 is influenced not only by the removal of corrosion products, but also by changes in water mobility, pore environment, and possible hydrogel residues. Among the investigated stones, Candoglia marble showed the least negative value, whereas Carrara marble and especially travertine exhibited a larger deviation from the untreated condition after cleaning. In the case of travertine, this behaviour may be consistent with its higher porosity, which can promote both the penetration of contaminants and the retention of water or gel residues within the pores. Therefore, the NMR recovery index should be considered as a semi-quantitative and complementary parameter rather than a direct measure of cleaning performance.

Overall, the NMR results indicate that the hydrogel treatment induces measurable changes in hydrogen mobility within the stone pore system. However, since the NMR measurement integrates areas with different degrees of cleaning and is influenced by water mobility and possible gel residues, the "lack of return" to the untreated values is consistent with partial removal and/or with a persistent modification of the surface proton environment. Nevertheless, these results are consistent with the FTIR, confirming the complementary information provided by portable NMR for evaluating cleaning treatments on stone materials.

Colorimetric Measurements

The colorimetric data show, in general, a certain variability, with reference to the different typologies of stone materials and the different formulations applied. The estimation of ΔE in Fig. 12, generally employed to assess the chromatic variation, was used in this case to prove the effect of the hydrogel on the cleaning. In general, all the formulations resulted effective in a removal of corrosion products from the surface. The cleaning, indeed, involved a decrease in the ΔE value of all the formulations and all the stone materials. The general trends observed for most of the measurements would correspond to a recovery of optical chromatic features, similar to those of unstained stone material. However, it is important to highlight that the measurement uncertainty is high in several of the tested area: this could derive from the surface characteristic of the stone materials, which could lead to the uneven distribution of the corrosion products and their consequent partial removal, and by the instrumental setup, which exploits a fiber optic, so it does not allow to acquire spectra on extended areas. For instance, in the case of Carrara, the ΔE value increased after cleaning in one area, but the measurement uncertainty would suggest that this measurement could be statistically inconsistent. Consequently, colorimetric measurements could be considered generally indicative of the cleaning performance, but they could not be applied to a deeper estimation in the comparison of the different formulation efficacy.

Overall, it seems that Candoglia marble exhibited the largest variations, indicating a higher sensitivity to the cleaning treatments. In contrast, Carrara marble showed lower ΔE values, suggesting greater chromatic stability. Travertine presented intermediate behaviour, likely related to its higher porosity. Among the tested formulations, gels containing LNPs generally produced lower ΔE values after cleaning, indicating a more controlled removal of surface deposits and a reduced impact on the substrate appearance.

ATR-FTIR Characterization of the Lignin-Based Hydrogel

In Fig. 13, the ATR-FTIR spectra of the three dry PVA-borax, PVA-LNPs and PVA-borax-LNPs hydrogels are shown. All peak assignments were made following the

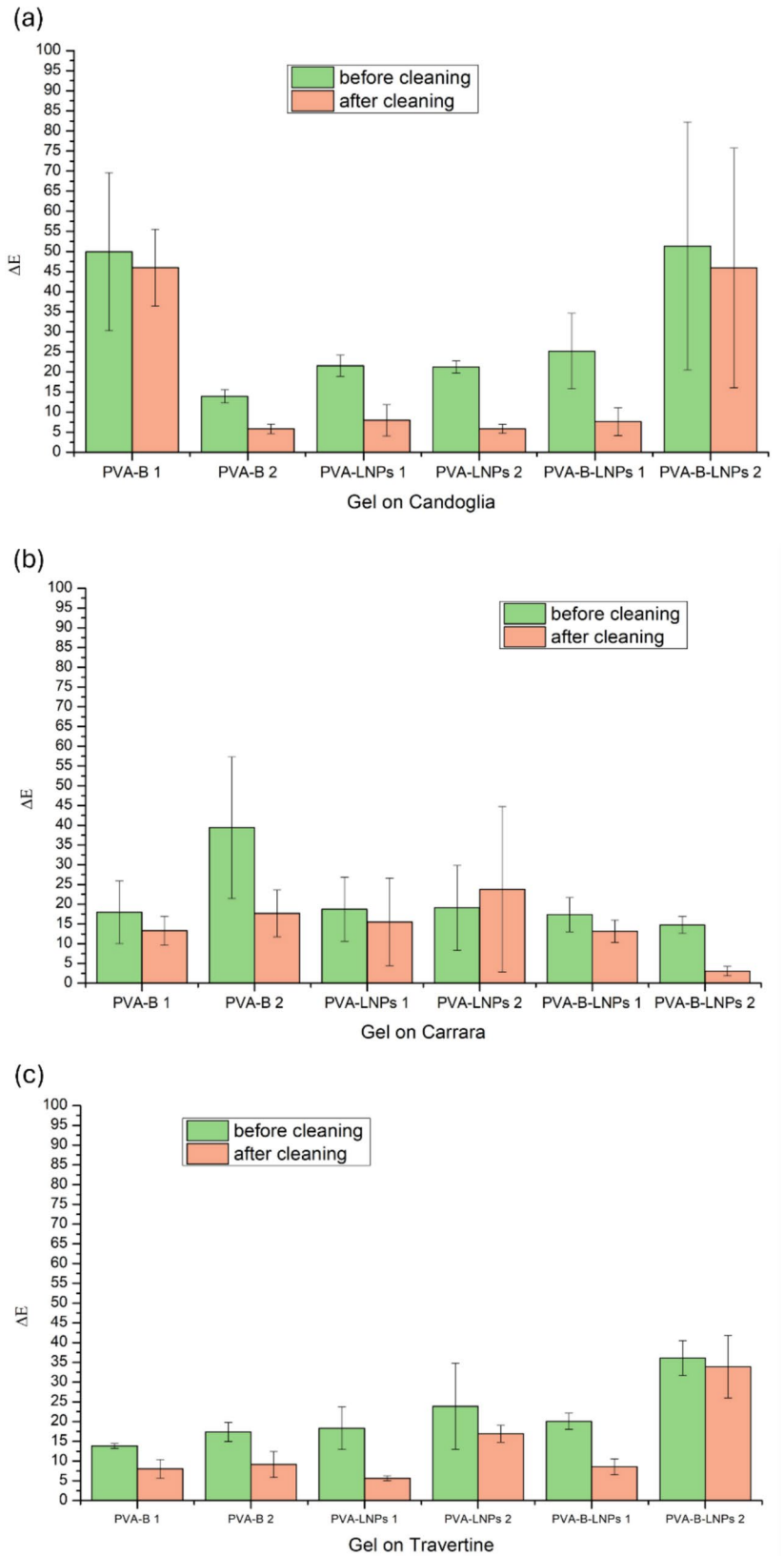

Fig. 12 Variation of ΔE measured in two different points of **a** Candoglia marble, **b** Carrara marble and **c** travertine surface before and after cleaning using the PVA-B, PVA-LNPs and PVA-B-LNPs hydrogel

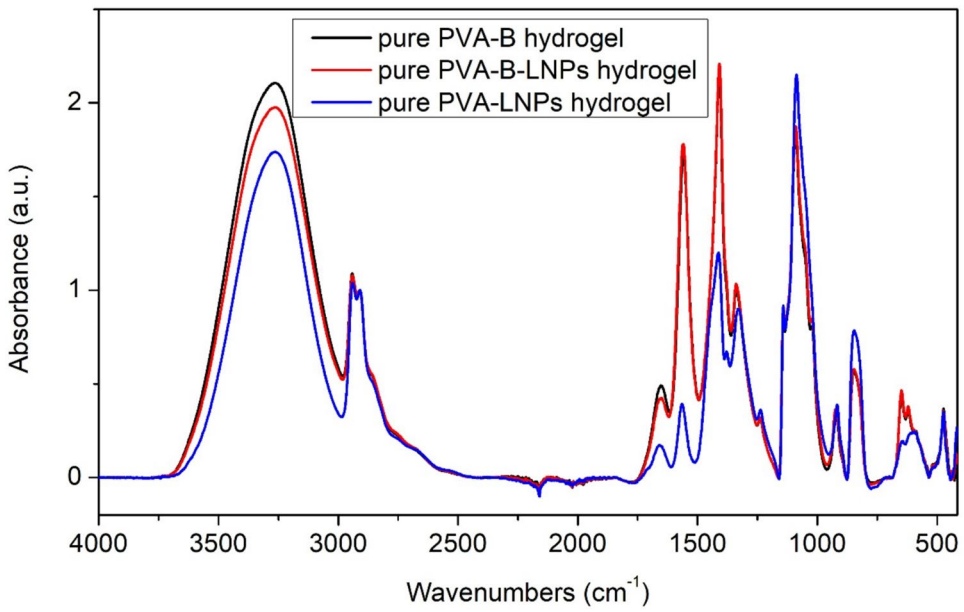

Fig. 13 ATR-FTIR spectrum of the dry PVA-borax, PVA-LNPs and PVA-borax-LNPs hydrogel. Comparison was made after intensity normalization (reference peak: C-H stretching signal at 2909 cm^{-1})

Table 5 ATR-FTIR peaks assignment for the dried pure hydrogel loaded with LNPs

Wavenumber (cm^{-1})	Assignment
833	CH bending
916	CH_2 rocking in PVA
1087	C–O deformation in secondary alcohols and aliphatic esters of lignin
1142	CO vibration (crystallinity) in PVA
1238	CH wagging of PVA
1339	B–O–C stretching (crosslinking/complexation)/phenolic hydroxyl groups of lignin
1381	Phenolic OH and aliphatic CH in methyl groups of lignin
1409	B–O–C stretching (crosslinking/complexation)/methoxyl groups of lignin
1566	Carbonyl group (C=O) stretching of lignin and of the acetate group residuals in PVA
1657	C=O stretching in conjugated carbonyl of lignin/O–H bending
2847	Asymmetric stretching vibration of the $–CH_2–$ groups
2909	C–H stretching
2937	C–H stretching

reference literature [34, 35, 63, 71, 94–101] and are reported in Table 5. The spectra show the main characteristics ascribable to the presence of PVA, borax and lignin. Particularly, the PVA-Borax spectrum presents the typical features ascribable to this typology of hydrogels. The bands at 846 and 922 cm^{-1} are attributable to C–C stretching and CH_2 bending, respectively. The intense peak at 1091 cm^{-1}, along with a lower intensity signal at 1022 cm^{-1}, is relatable to PVA C–O stretching, while the sharp peak at 1143 cm^{-1} is assigned to C–C stretching of PVA. The peak at 1238 cm^{-1}, along with a shoulder around 1380 cm^{-1}, is assigned to CH_2 wagging [36]. The bands at 1339 and 1409 cm^{-1} are attributed to the tetrahedral and trigonal, respectively, complex-crosslinking of PVA, in this case with borate (B–O–C stretching relaxation) [34, 36, 65, 66, 81, 82]. The intense peak at 1558 cm^{-1} is ambiguously assigned in literature: in some cases, it is considered indicative of carbonyl residual moieties of poly vinyl acetate precursor, in some other cases it is assigned to C=C monomer residuals. However, its appearance in the spectrum of pure PVA powder would be consistent with these hypotheses, while it cannot be considered indicative of interaction with the cross-linkers. Finally, signals at 1652 and 3261 cm^{-1} are attributable to OH bending and stretching, respectively, while, in the C-H stretching range, the shoulder at 2850 cm^{-1} and the peaks at 2910 and 2941 cm^{-1} appear.

For the PVA-LNPs formulation, a general similarity in the spectral pattern is identified, with some differences attributable to the loading of LNPs instead of borax. In particular, the peak at 922 cm^{-1} shifts at the 917 cm^{-1}, while the broadening of the peak at 1091 cm^{-1}, with the consequent disappearance of the signal at 1022 cm^{-1}, could be attributed to the overlap

with the CH aromatic ring deformation and, moreover, to the differentiation of C–O stretching deriving from the interaction with the various functional groups in lignin. Particularly interesting is the shift of the band of tetrahedral crosslinking of PVA to 1326 cm^{-1}, which could reflect the difference in complexation, while the band at 1409 cm^{-1} varies in shape, with a new shoulder around 1440 cm^{-1}, and decreases in intensity. A new signal appears at 1378 cm^{-1}, assignable to phenolic OH and aliphatic CH in methyl groups of lignin, which confirms its loading in the gel, along with a shoulder around 1706 cm^{-1}, assignable to esters in LNPs. Finally, the intensity of the band at 1558 cm^{-1} strongly decreases, along with the O–H bending and stretching band. These variations confirm a decrease of free hydroxy groups, deriving from the interaction between PVA and LNPs. In the C–H stretching range, no evident changes attributable to organic compounds besides the PVA are clearly observable.

For the PVA-borax-LNPs hydrogel, it is interesting to notice that the general spectral pattern corresponds to the analogue of PVA-borax, suggesting that the borax is the main cross-linker. However, some differences could be envisaged, which are attributable to the interaction of lignin. In particular, a slight broadening of the bands in the 950–1160 cm^{-1} (C–O stretching) and 1250–1490 cm^{-1} (C–H wagging and PVA cross-linking) suggest the differentiation of interaction, while the O–H stretching at 3261 cm^{-1} is characterized by an intermediate intensity compared to the other gels, suggesting LNPs addition resulted in the actual decrease of available hydroxy groups. The most interesting information derives from the variation of a series of peak intensity ratios (Table 6). The intensity ratio between the peak at 1091 cm^{-1} and the analogue at 1652 cm^{-1} highlights how the number of free O–H strongly decreases in comparison to the C–O bonds in PVA-LNPs formulation in comparison to the analogue with borax, deriving from the interaction with the functional groups of lignin. In the formulation with both the crosslinker, this ratio is higher than in PVA-borax and strongly lower than in PVA-LNPs, confirming that the borax is the principal crosslinker, but LNPs increase have an additive effect on the formation of the network. This is also confirmed by the ratios between the bands at 1338 and 1410 cm^{-1}, indicative of PVA complexation, and the O–H bending: in both the cases, the PVA-borax-LNPs show a combination effect deriving from the presence of the two cross-linkers. An interesting information, finally, derives from the ratio between the bands at 922 and 846 cm^{-1} [102]. The intensity ratio between these two bands, in fact, increases with the number of syndiotactic portions in the polymers. Interestingly, the addition of both the cross-linkers corresponds to a higher syndiotactic arrangement.

Table 6 Variations of ATR-FTIR peaks intensity ratio along the three different hydrogel formulations

Formulation	I_{1091}/I_{1652}	I_{1339}/I_{1652}	I_{1409}/I_{1652}	I_{922}/I_{846}
PVA-borax	3.74	2.04	4.40	0.58
PVA-LNPs	12.38	5.25	6.97	0.50
PVA-borax-LNPs	4.42	2.44	5.20	0.63

The ATR-FTIR spectrum collected on the dry pure PVA-borax hydrogel, PVA-LNPs hydrogel and PVA-borax-LNPS hydrogel was compared with the spectra collected on each dry layer of gel after being peeled off from Candoglia marble, Carrara marble and travertine. The comparison is reported in Fig. 14 for the PVA-B, in Fig. 15 for the

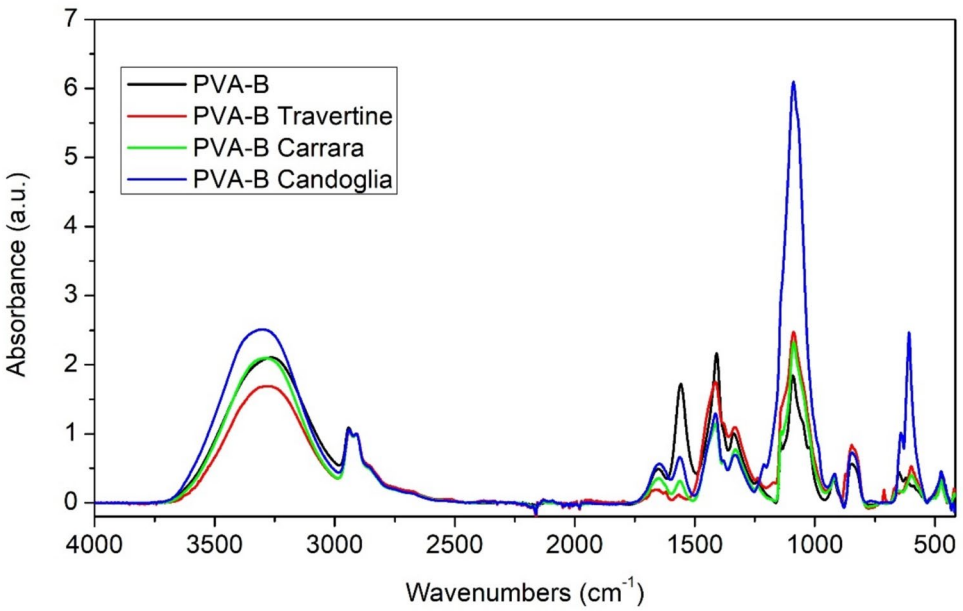

Fig. 14 Comparison of ATR spectra acquired on the dry PVA-B layer before and after being used to clean the three lithotypes

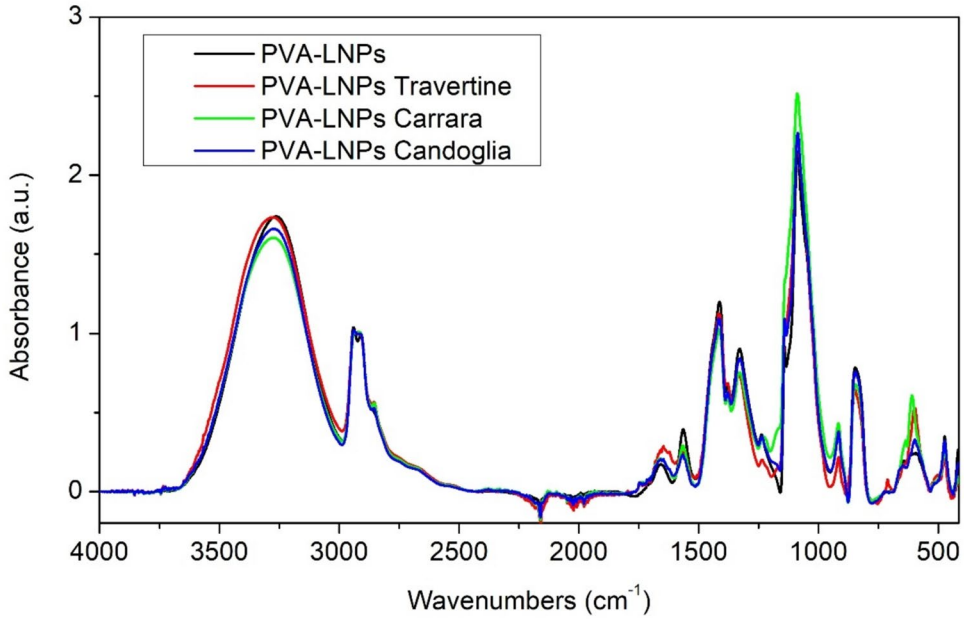

Fig. 15 Comparison of ATR spectra acquired on the dry PVA-LNPs layer before and after being used to clean the three lithotypes

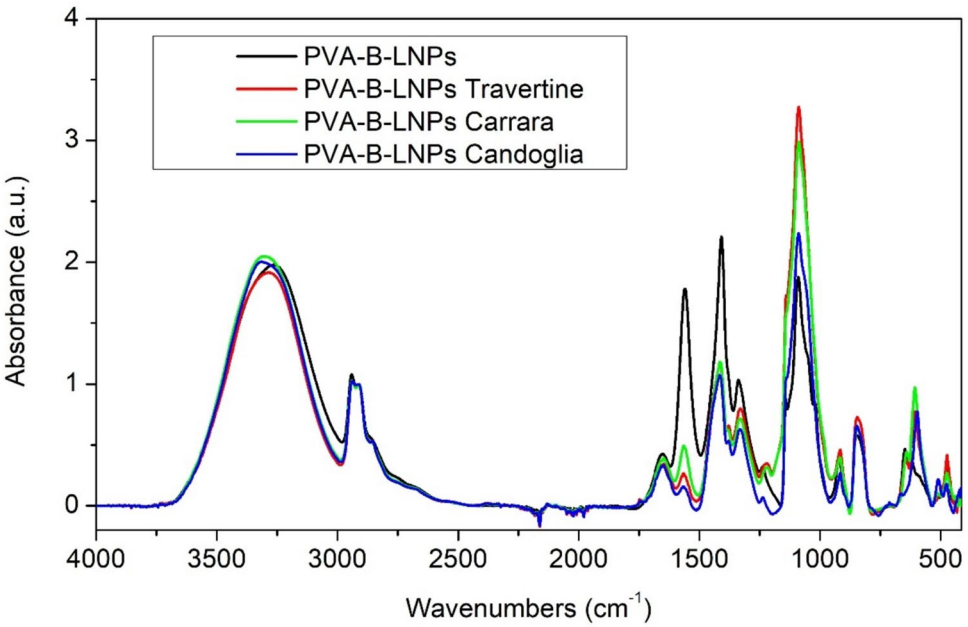

Fig. 16 Comparison of ATR spectra acquired on the dry PVA-B-LNPs layer before and after being used to clean the three lithotypes

PVA-LNPs and in Fig. 16 for the PVA-B-LNPs,, after intensity normalization (reference peak: C-H stretching signal at 2909 cm^{-1}). The appearance of low intensity bands around 600–612 and 630–650 cm^{-1} could be considered indicative of the formation of Cu(II)-PVA complexes (Cu(II)–O bond) and it can be used to compare the interaction of the different gels. In the case of PVA-borax, no signal is evident at 600 cm^{-1}, while it appears in all the gels after cleaning, among which it is particularly evident in the case of Candoglia marble. In the case of PVA-LNPs, a low intensity band is present in the pure gel, but after cleaning the signal increases in intensity remarkably for all the lithotypes. The same increase in intensity is observable in the PVA-borax-LNPs formulation. In all the spectra for the gels after cleaning, moreover, the peak at 1091 cm^{-1} increases in intensity, even if with different trends for every gel with reference to the typology of stone. Another evident variation is related to the peak at 1566 cm^{-1} [34]: in all the gels used for the cleaning, the apparent intensity of this signal decreases, while, for all the hydrogels, the band of O–H stretching around 3261 cm^{-1} shifts to higher wavenumbers (between 3280 and 3320 cm^{-1}) after cleaning, which is indicative of the

rearrangement of hydroxy groups after interaction of the gel with the metals.

Some spectral features are subjected to different variations in the different gels. For instance, in the case of PVA-borax formulation, the signal at 1238 cm^{-1}, attributable to C-H wagging in PVA, is in unvaried for the cleaning of travertine and Carrara marble, while it disappears for the Candoglia marble and a new band at 1211 cm^{-1} appears. For the PVA-LNPs hydrogel, instead, the signal at 1238 cm^{-1} is still visible in travertine and Candoglia spectra with the shoulder at 1211 cm^{-1}, while for the Carrara the band broadens remarkably and a new shoulder around 1170 cm^{-1} is observable. Finally, in the case of PVA-borax-LNPs, these variations are clearly observable for both travertine and Carrara, while Candoglia is unaffected. These changes in the region 1170–1238 cm^{-1} compared to the reference hydrogels indicate the entrapment of copper sulphates [86] into the matrix. It is also important to highlight that both the signals at 600 and 1170–1238 cm^{-1} would confirm a trend: if PVA-borax are able to complex copper products only in the case of Candoglia, the PVA-LNPs formulation is able to extract them from all the lithotypes, while the PVA-borax-LNPs has an intermediate behavior. This hypothesis is also proved by the O–H bending signals and the appearance of a band around 1620 cm^{-1}, attributable to the bending of a chemically different hydroxy group. This band is not visible in the case of PVA-borax formulation, with the exception of the travertine cleaning, while it is observable for the cleaning of all the stones in the case of PVA-LNPs and it appears as a shoulder/broadening in the case of PVA-borax-LNPs formulation.

Insights regarding the cleaning mechanism could be extracted from the evaluation of the intensity ratios (Table 7). In general, the increase in the intensity ratio I_{1091}/I_{1652} would be consistent with the interaction of free O–H groups and the metals. On the contrary, the decrease of PVA chelation band ratios (I_{1339}/I_{1652} and I_{1409}/I_{1652}) would correspond to breaking of PVA-crosslinker interactions after contact with the metal. For the PVA-B film, the interaction with the stained stone surface corresponds to a great increase in the C–O/O–H intensity ratio I_{1091}/I_{1652}, while the analogues for the PVA complexation bands result increasing only in the case of travertine. For the PVA-LNPs, instead, the I_{1091}/I_{1652} results are mostly unaffected or decrease only in the case of travertine, while the complexation bands generally decrease, with the highest variation for travertine and the lowest for Candoglia marble. These data suggest that, in the first case, the extraction of metals is due to chelation through the free hydroxy groups in the polymer, which are not already coordinating boron atoms, while, for the second formulation, the chelation with copper could involve principally the coordination centres involving the polymer and the LNPs. In the case of the PVA-B-LNPs, indeed, the behaviour is intermediate, with a general increase in intensity for the I_{1091}/I_{1652} ratio and a decrease for the intensity ratios involving the complexation bands. The addition of LNPs to PVA-borax could correspond to a combined chelating mechanism, involving both the unbound O–H groups of the polymer and the LNPs functionalities.

It is interesting to observe that the greatest variations of the peak ratio I_{1091}/I_{1652} were observed for the travertine cleaning, which would correspond to better cleaning performances tested for this lithotype, as assessed by the Recovery Index and supported by NMR. For the travertine, moreover, the intensity ratios would suggest hypotheses about the cleaning mechanism. In the PVA-B formulation, the increase of all the ratios involving the O–H band would be consistent with the involvement of these functional groups in the coordination of the metals: the free hydroxy groups are in charge for the complexation of the metal. In the PVA-LNPs, instead, the decrease of these ratios would be attributable to the role of LNPs, with the breaking of their coordination to the PVA in favour of new interaction with the metals. Finally, in the PVA-B-LNPs, it is possible to observe an intermediate behavior, where the I_{1091}/I_{1652} increases for the metal coordination through the free hydroxy groups in PVA, while the complexation band ratios decrease because of the involvement of LNPs moieties. The comparable variation for the Carrara and Candoglia marbles, instead, agree with their similar values for the Recovery Index. In particular, for these lithotypes, in the case of PVA-LNPs formulation the decrease of the ratio intensity of the PVA complexation band is less evident than in the case of travertine, which would suggest that the LNPs have a less pronounced role in the cleaning for these stone materials. The slightly higher decrease for the I_{1091}/I_{1652} ratio in the case of Candoglia, moreover, would be coherent with the slightly higher Recovery Index observed for this marble, in comparison to Carrara stone. On the opposite, for the PVA-B-LNPs formulation, the decrease of the ratios is more marked for the two marble

Table 7 Variations of ATR-FTIR peaks intensity ratio along the three different hydrogel formulations after being used to clean the three different lithotypes surface

Formulation	Lithotype	I_{1091}/I_{1652}	I_{1339}/I_{1652}	I_{1409}/I_{1652}	I_{922}/I_{846}
PVA-borax	Travertine	12.95	5.88	9.41	0.50
	Carrara	6.58	2.17	3.22	0.51
	Candoglia	10.73	1.22	2.28	0.58
PVA-LNPs	Travertine	7.78	2.55	3.92	0.34
	Carrara	11.99	3.59	4.89	0.64
	Candoglia	11.12	4.12	5.36	0.50
PVA-borax-LNPs	Travertine	9.50	2.32	3.39	0.63
	Carrara	7.62	1.82	3.01	0.62
	Candoglia	6.72	1.89	3.23	0.41

lithotypes than travertine. Consequently, in the case of the two marbles the combination of borax and LNPs would have a synergic effect, even consistent with the increase of the Recovery Index related to PVA-B-LNPs formulation, with reference to its analogues, for all the lithotypes. Finally, the observed variations confirm that, in general, the PVA-B-LNPs formulation could be considered the best performing, consistently with ER-FTIR data.

Overall Cleaning Performance, Limitations and Future Perspectives of Lignin-Based Hydrogel

The cleaning performance of the lignin-based hydrogel, used in this study, varies depending on the lithotype, reflecting differences in the petrophysical properties of the stones, such as porosity and surface characteristics. The three stones used have a similar chemical composition (mainly $CaCO_3$), but they significantly differ in their pore structure [64, 65, 67, 68, 70]. Candoglia marble and Carrara marble are compact crystalline marbles characterized by very low porosity and limited pore connectivity. Therefore, the artificially deposited metal corrosion products tend to remain mostly confined to the outermost surface layer of the stone. Under these conditions, the lignin-based hydrogel can interact more effectively with the contaminants located at the stone-gel interface, facilitating their removal. In contrast, travertine is a highly porous carbonate rock characterized by a larger pore volume, higher pore connectivity, and a more heterogeneous pore-size distribution [40, 64, 65, 67, 103, 104]. These structural characteristics favour a deeper penetration of the metal salt solution during the artificial staining process. As a result, corrosion products can accumulate not only at the surface but also within the interconnected pore network of travertine, as confirmed by portable NMR that collects the signal coming from the surface and the first 2 mm below the surface compared to FTIR, which investigates a surface thickness of a few tens of micrometres. This behaviour likely explains the lower cleaning efficiency observed for travertine using NMR and ER-FTIR. Moreover, the higher water retention capacity of travertine may influence the interaction between the hydrogel and the substrate. The presence of retained moisture within the pore system, detected by portable NMR as a variation in the T_2 peak intensity (associated with changes in the pore water environment) after contact with the gel, may limit the extraction of metal ions and reduce the effective diffusion of contaminants toward the hydrogel matrix. In addition, since the hydrogel mainly acts at the stone-gel interface, its ability to extract corrosion products from deeper pore systems may be limited. All these factors provide a plausible explanation for the lower cleaning performance obtained for travertine compared to the more compact marbles using visual inspection, NMR and ER-FTIR. Nevertheless, the recovery index calculated from the FTIR carbonate band shows higher values for travertine. This suggests that the lignin-based hydrogel is effective at the stone surface interface, promoting the recovery of the carbonate spectral features, although it is less effective in removing corrosion products that have penetrated into the internal pore network.

The results obtained from ATR-FTIR in this study suggest that lignin into a hydrogel matrix effectively participate in the metal ions capture from contaminated carbonate stones. For instance, the decrease in intensity of the complexation bands of PVA in some FTIR spectra indicates that intermolecular interactions between the nano-lignin and the polymer break, probably because of the contact with the metal species on the surface. The comparison of intensity ratios for the PVA bands in the different formulations, before and after the cleaning, would highlight that the action could be synergic, especially in the case of the marbles. Nonetheless, the present investigation should be considered preliminary, and several limitations must be acknowledged.

First, the brownish stains observed on the stone surfaces, likely associated with copper oxides, mixed copper hydroxyl-salts and possibly iron-bearing compounds derived from the metal coins, were only partially affected by the hydrogel treatment. As indicated by ER-FTIR spectra and visual inspection, these compounds persisted on the surface even after repeated applications of the gel, while the removal of greenish corrosion products such as copper sulphates and chlorinated copper compounds was more effective. This behaviour suggests that the interaction between the lignin functional groups and different corrosion products may vary depending on the chemical nature and stability of the compounds present on the stone surface. Future investigations should therefore focus on optimizing the chemical affinity of the lignin-based hydrogel. This could be achieved by modifying the lignin content or by introducing additional functional groups, through chemical modification of nano-lignin, capable of enhancing complexation with metal oxides. Another important limitation concerns the inhomogeneous surface cleaning and limited penetration depth of the hydrogel within the stone pore system. Visual inspection, FTIR, NMR, and colorimetric measurements revealed that the hydrogel action was not uniform across the stone surface, with areas showing effective removal of corrosion products and other zones where residues remained detectable. Moreover, portable NMR measurements probe a region approximately 2 mm below the surface and showed only a partial recovery of the relaxation times after cleaning, suggesting that corrosion products may remain in deeper pores or that residual modifications of the hydrogen environment persist after treatment. The cleaning performance

of the lignin-based hydrogel depends on several factors, including the irregular distribution of corrosion products, differences in stone surface roughness and porosity (as for travertine), and variations in the contact between the hydrogel layer and the substrate. Moreover, its ability of extracting metal ions from deeper pore networks was limited. In future studies, the optimization of the hydrogel rheological and mechanical properties, as well as its porosity and water retention properties, will be necessary to enhance its adhesion and conformability to irregular stone surfaces and to improve ion diffusion and transport within the hydrogel network.

Conclusions

This study proposes a sustainable alternative to conventional chelator-based gels for stone artworks cleaning. In this approach, waste lignin is valorised through its conversion into lignin nanoparticles incorporated into a PVA–borax hydrogel matrix, providing a bio-based material with potential metal-binding capability. The incorporation of lignin nanoparticles into the hydrogel network allows the formation of a transparent gel suitable for application on white stone substrates without leaving any visible stains. ATR-FTIR confirmed that lignin functional groups participate, together with the other gel components, to chemical entrapment of metal corrosion products and that the cleaning action could be synergic, especially in the case of the marbles, an aspect worth of further deepening. The cleaning performance was found to depend on both the lithotype and the nature of the corrosion products. In particular, greenish corrosion compounds associated with copper sulphates and chlorinated copper species were more effectively removed, whereas brownish stains, likely related to copper oxides and iron-containing phases, were less affected by the treatment. Moreover, the efficiency of the cleaning process is influenced by the petrophysical properties of the stone substrates. In more porous materials such as travertine, corrosion products may penetrate into the pore network, limiting the extraction capability of the hydrogel acting mainly at the stone–gel interface. The combined use of portable ER-FTIR and portable NMR proved to be a valuable non-invasive diagnostic approach for monitoring the cleaning process. These complementary techniques allowed the evaluation of both chemical changes at the surface and modifications in the pore water environment associated with contamination and cleaning treatments.

Overall, the results indicate that lignin-based hydrogels represent a promising sustainable material for stone conservation. Further studies should focus on improving the formulation by increasing the lignin nanoparticle content, modifying the polymer network to enhance mechanical properties, and potentially replacing borax with greener cross-linking agents to further improve the sustainability of the system. Finally, a deeper understanding of the interaction mechanisms between lignin, metals and stone substrates is required, together with further evaluation of the performance of these hydrogels on real cultural heritage surfaces.

Supplementary Information The online version contains supplementary material available at https://doi.org/10.1007/s12649-026-03603-1.

Acknowledgements The authors thank Dr. Simona Sennato for her scientific support during the DLS experiments.

Author Contributions All authors contributed to the study conception and design. Material preparation, data collection and analysis were performed by Valeria Stagno, Melania Di Fazio, Alessandro Ciccola and Rosaceleste Zumpano. The first draft of the manuscript was written by Valeria Stagno and all authors commented on previous versions of the manuscript. All authors read and approved the final manuscript.

Funding Open access funding provided by Università degli Studi di Roma La Sapienza within the CRUI-CARE Agreement. This work was supported by the*Avvio alla Ricercaprogram of Sapienza University of Rome, call for proposals n. 36805 and n. 39677, within the project "Development of Nuclear Magnetic Resonance protocols for the characterization and monitoring of lignin nanoparticle-based consolidants for submerged archaeological wood" and "Synthesis of ad-hoc Lignin Nanoparticles (LNPs) for waterlogged wood consolidation and development of innovative NMR protocols for their characterization".*

Data Availability The data is included in the article and presented in tables and Figures.

Declarations

Conflict of interests The authors have no relevant financial or non-financial interests to disclose.

References

1. Rico-Garcìa, D., Ruiz-Rubio, L., Pérez-Alvarez, L., Hernández-Olmos, S.L., Guerrero-Ramírez, G.L., Vilas-Vilela, J.L.: Lignin-based hydrogels : synthesis and applications. Polymers **12**(1), 81 (2020). https://doi.org/10.3390/polym12010081
2. Hachimi Alaoui, C., Réthoré, G., Weiss, P., Fatimi, A.: Sustainable biomass lignin-based hydrogels: a review on properties,

formulation, and biomedical applications. Int. J. Mol. Sci. **24**(17), 13493 (2023). https://doi.org/10.3390/ijms241713493
3. Mignardi, S., Archilletti, L., Medeghini, L., De Vito, C.: Valorization of eggshell biowaste for sustainable environmental remediation. Sci. Rep. **10**(1), 1–10 (2020). https://doi.org/10.1038/s41598-020-59324-5
4. Amusa, A.A., Ahmad, A.L., Adewole, J.K.: Mechanism and compatibility of pretreated lignocellulosic biomass and polymeric mixed matrix membranes: a review. Membranes **10**(12), 370 (2020). https://doi.org/10.3390/membranes10120370
5. Anwar, Z., Gulfraz, M., Irshad, M.: Agro-industrial lignocellulosic biomass a key to unlock the future bio-energy: a brief review. J. Radiat. Res. Appl. Sci. **7**(2), 163–173 (2014). https://doi.org/10.1016/j.jrras.2014.02.003
6. Vásquez-Garay, F., Carrillo-Varela, I., Vidal, C., Reyes-Contreras, P., Faccini, M., Mendonça, R.T.: A review on the lignin biopolymer and its integration in the elaboration of sustainable materials. Sustainability **13**(5), 2697 (2021). https://doi.org/10.3390/su13052697
7. Chanoca, A., de Vries, L., Boerjan, W.: Lignin engineering in forest trees. Front. Plant Sci. (2019). https://doi.org/10.3389/fpls.2019.00912
8. Argyropoulos, D.D.S., et al.: Kraft lignin: a valuable, sustainable resource, opportunities and challenges. Chemsuschem **16**(23), e202300492 (2023). https://doi.org/10.1002/cssc.202300492
9. Bakshi, M.I., et al.: Recent advances in lignin from forest residue for hydrogel application. Biomass Convers. Biorefinery **15**(8), 11475–11491 (2025). https://doi.org/10.1007/s13399-024-05973-9
10. Stafford, W., et al.: Forestry biorefineries. Renew. Energy **154**, 461–475 (2020). https://doi.org/10.1016/j.renene.2020.02.002
11. Mohammed, N.I., Kabbashi, N., Alade, A.: Significance of agricultural residues in sustainable biofuel development. In: Agricultural Waste and Residues, Aladjadjiyan, A., (ed.) IntechOpen, London (2018)
12. Isikgor, F.H., Becer, C.R.: Lignocellulosic biomass: a sustainable platform for the production of bio-based chemicals and polymers. Polym. Chem. **6**(25), 4497–4559 (2015). https://doi.org/10.1039/c5py00263j
13. Cheng, S., Yuan, Z., Leitch, M., Anderson, M., Xu, C.C.: Highly efficient de-polymerization of organosolv lignin using a catalytic hydrothermal process and production of phenolic resins/adhesives with the depolymerized lignin as a substitute for phenol at a high substitution ratio. Ind. Crops Prod. **44**, 315–322 (2013). https://doi.org/10.1016/j.indcrop.2012.10.033
14. Aro, T., Fatehi, P.: Production and application of lignosulfonates and sulfonated lignin. Chemsuschem **10**(9), 1861–1877 (2017). https://doi.org/10.1002/cssc.201700082
15. Zakzeski, J., Bruijnincx, P.C.A., Jongerius, A.L., Weckhuysen, B.M.: The catalytic valorization of lignin for the production of renewable chemicals. Chem. Rev. **110**(6), 3552–3599 (2010). https://doi.org/10.1021/cr900354u
16. Fache, M., Boutevin, B., Caillol, S.: Vanillin production from lignin and its use as a renewable chemical. ACS Sustain. Chem. Eng. **4**(1), 35–46 (2016). https://doi.org/10.1021/acssuschemeng.5b01344
17. Jiang, G., Nowakowski, D.J., Bridgwater, A.V.: A systematic study of the kinetics of lignin pyrolysis. Thermochim. Acta **49**(1–2), 61–66 (2010). https://doi.org/10.1016/j.tca.2009.10.003
18. Saadan, R., Hachimi Alaoui, C., Ihammi, A., Chigr, M., Fatimi, A.: A brief overview of lignin extraction and isolation processes: from lignocellulosic biomass to added-value biomaterials. Environ. Earth Sci. Proc. **31**(1), 3 (2024). https://doi.org/10.3390/eesp2024031003
19. Raza, M., et al.: Extraction and characterization of lignin from lignocellulose biomass using citric acid and fructose-based NADES. Int. J. Biol. Macromol. **321**, 146497 (2025). https://doi.org/10.1016/j.ijbiomac.2025.146497
20. Siddique, M., Soomro, S.A., Aziz, S.: Characterization and optimization of lignin extraction from lignocellulosic biomass via green nanocatalyst. Biomass Convers. Biorefinery **14**(22), 28523–28531 (2024). https://doi.org/10.1007/s13399-022-03598-4
21. Dandash, A.A., Abu-Jdayil, B., Tannous, J.H.: Lignin extraction from various biomass sources: a comprehensive review of characteristics, applications, and future prospects. Chem. Rec. **25**(8), e202500045 (2025). https://doi.org/10.1002/tcr.202500045
22. Abolore, R.S., Jaiswal, S., Jaiswal, A.K.: A comprehensive review on sustainable lignin extraction techniques, modifications, and emerging applications. Ind. Crops Prod. **235**, 121696 (2025). https://doi.org/10.1016/j.indcrop.2025.121696
23. Verma, D., Jha, M.K., Kumar, S.: A comprehensive review on lignin extraction from lignocellulosic biomass, and nano-lignin synthesis and modification for potential applications. Can. J. Chem. Eng. (2025). https://doi.org/10.1002/cjce.70151
24. Norgren, M., Edlund, H.: Lignin: recent advances and emerging applications. Curr. Opin. Colloid Interface Sci. **19**(5), 409–416 (2014). https://doi.org/10.1016/j.cocis.2014.08.004
25. Chakar, F.S., Ragauskas, A.J.: Review of current and future softwood kraft lignin process chemistry. Ind. Crops Prod. **20**(2), 131–141 (2004). https://doi.org/10.1016/j.indcrop.2004.04.016
26. Domínguez-Robles, J., Cárcamo-Martínez, Á., Stewart, S.A., Donnelly, R.F., Larrañeta, E., Borrega, M.: Lignin for pharmaceutical and biomedical applications: could this become a reality? Sustain. Chem. Pharm. **18**, 100320 (2020). https://doi.org/10.1016/j.scp.2020.100320
27. Mariana, M., et al.: A current advancement on the role of lignin as sustainable reinforcement material in biopolymeric blends. J. Mater. Res. Technol. **15**, 2287–2316 (2021). https://doi.org/10.1016/j.jmrt.2021.08.139
28. Liu, Q., Zhang, H., Ren, H., Zhai, H.: Structural analysis of light-colored separated lignin (lignocresol) and its antioxidant properties. Int. J. Biol. Macromol. (2022). https://doi.org/10.1016/j.ijbiomac.2021.12.144
29. Thakur, V.K., Thakur, M.K.: Recent advances in green hydrogels from lignin: a review. Int. J. Biol. Macromol. **72**, 834–847 (2015). https://doi.org/10.1016/j.ijbiomac.2014.09.044
30. Zhao, W., Simmons, B., Singh, S., Ragauskas, A., Cheng, G.: From lignin association to nano-/micro-particle preparation: extracting higher value of lignin. Green Chem. **18**(21), 5693–5700 (2016). https://doi.org/10.1039/c6gc01813k
31. Thulluri, C., Pinnamaneni, S.R., Shetty, P.R., Addepally, U.: Synthesis of lignin-based nanomaterials/nanocomposites: recent trends and future perspectives. Ind. Biotechnol. **12**(3), 153–160 (2016). https://doi.org/10.1089/ind.2015.0022
32. Dragan, E.S.: Design and applications of interpenetrating polymer network hydrogels. a review. Chem. Eng. J. **243**, 572–590 (2014). https://doi.org/10.1016/j.cej.2014.01.065
33. Akhtar, M.F., Hanif, M., Ranjha, N.M.: Methods of synthesis of hydrogels: a review. Saudi Pharm. J. **24**(5), 554–559 (2016). https://doi.org/10.1016/j.jsps.2015.03.022
34. Al-Emam, E., Soenen, H., Caen, J., Janssens, K.: Characterization of polyvinyl alcohol-borax/agarose (PVA-B/AG) double network hydrogel utilized for the cleaning of works of art. Herit. Sci. **8**(1), 1–14 (2020). https://doi.org/10.1186/s40494-020-00447-3
35. Giuliani, L., et al.: Multi-technique assessment of chelators-loaded PVA-Borax gel-like systems performance in cleaning of stone contaminated with copper corrosion products. Gels (2024). https://doi.org/10.3390/gels10070455
36. Angelova, L.V., Berrie, B.H., De Ghetaldi, K., Kerr, A., Weiss, R.G.: Partially hydrolyzed poly(vinyl acetate)-boraxbased

gel-like materials for conservation of art: characterization and applications. Stud. Conserv. **60**(4), 227–244 (2015). https://doi.org/10.1179/2047058413Y.0000000112
37. Riedo, C., Rollo, G., Chiantore, O., Scalarone, D.: Detection and identification of possible gel residues on the surface of paintings after cleaning treatments. Heritage **4**(1), 304–315 (2021). https://doi.org/10.3390/heritage4010019
38. Riedo, C., Caldera, F., Poli, T., Chiantore, O.: Poly(vinylalcohol)-borate hydrogels with improved features for the cleaning of cultural heritage surfaces. Herit. Sci. **3**(1), 23 (2015). https://doi.org/10.1186/s40494-015-0053-2
39. Carretti, E., et al.: A new family of high viscosity polymeric dispersions for cleaning easel paintings. J. Cult. Herit. **11**(4), 373–380 (2010). https://doi.org/10.1016/j.culher.2010.04.002
40. Stagno, V., Ciccola, A., Curini, R., Postorino, P., Favero, G., Capuani, S.: Non-invasive assessment of PVA-borax hydrogel effectiveness in removing metal corrosion products on stones by portable NMR. Gels **7**(4), 265 (2021). https://doi.org/10.3390/gels7040265
41. Alemam, E.: Cleaning of wall paintings by polyvinyl alcohol–borax/agarose (PVA–B/AG) double network hydrogels: characterization, assessment, and applications (2021)
42. Stagno, V., Genova, C., Zoratto, N., Favero, G., Capuani, S.: Single-sided portable NMR investigation to assess and monitor cleaning action of PVA-borax hydrogel in travertine and Lecce Stone. Molecules **26**(12), 3697 (2021). https://doi.org/10.3390/molecules26123697
43. Angelova, L.V., Matarrese, C., Fratini, E., Weiss, R.G., Dei, L., Carretti, E.: Chelating agents in aqueous, partially-hydrolyzed, poly(vinyl acetate) dispersions crosslinked with borax. Physicochemical characterization and an application. Colloids Surf A Physicochem Eng Asp **556**, 61–71 (2018). https://doi.org/10.1016/j.colsurfa.2018.07.044
44. Angelova, L.V.: Gels from borate-crosslinked partially hydrolyzed poly(vinyl acetate)s: characterization of physical and chemical properties and applications in art conservation, Georgetown University (2013)
45. Chelazzi, D., Fratini, E., Giorgi, R., Mastrangelo, R., Rossi, M., Baglioni, P.: Gels for the cleaning of works of art. ACS Symp. Ser. **1296**, 291–314 (2018). https://doi.org/10.1021/bk-2018-1296.ch015
46. Lin, H.L., Liu, Y.F., Yu, T.L., Liu, W.H., Rwei, S.P.: Light scattering and viscoelasticity study of poly(vinyl alcohol)-borax aqueous solutions and gels. Polymer **46**(15), 5541–5549 (2005). https://doi.org/10.1016/j.polymer.2005.04.074
47. Mazzuca, C., et al.: Polyvinyl alcohol based hydrogels as new tunable materials for application in the cultural heritage field. Colloids Surf. B Biointerfaces **188**, 110777 (2020). https://doi.org/10.1016/j.colsurfb.2020.110777
48. Lawrence, M.B., Desa, J.A.E., Aswal, V.K.: Reentrant behaviour in polyvinyl alcohol-borax hydrogels. Mater. Res. Express (2018). https://doi.org/10.1088/2053-1591/aaa6e6
49. Berlangieri, C., et al.: Chelators confined into 80pvac-borax highly viscous dispersions for the removal of gypsum degradation layers. Pure Appl. Chem. **89**(1), 97–109 (2017). https://doi.org/10.1515/pac-2016-0815
50. Domingues, J., Bonelli, N., Giorgi, R., Baglioni, P.: Chemical semi-IPN hydrogels for the removal of adhesives from canvas paintings. Appl. Phys. A **114**(3), 705–710 (2014). https://doi.org/10.1007/s00339-013-8150-0
51. Baglioni, P., Chelazzi, D., Giorgi, R.: Nanorestart: nanomaterials for the restoration of works of art. Herit. Sci. **9**(1), 5 (2021). https://doi.org/10.1186/s40494-020-00477-x
52. Al-Emam, E., Motawea, A.G., Janssens, K., Caen, J.: Evaluation of polyvinyl alcohol–borax/agarose (PVA–B/AG) blend hydrogels for removal of deteriorated consolidants from ancient Egyptian wall paintings. Herit. Sci. **7**, 22 (2019). https://doi.org/10.1186/s40494-019-0264-z
53. Khaksar-Baghan, N., Koochakzaei, A., Hamzavi, Y.: An overview of gel-based cleaning approaches for art conservation. Herit. Sci. **12**(1), 248 (2024). https://doi.org/10.1186/s40494-024-01369-0
54. Baglioni, P., Chelazzi, D., Giorgi, R.: Nanotechnologies in the conservation of cultural heritage: a compendium of materials and techniques, 1st ed. Springer Dordrecht, Firenze (2014)
55. Nowack, B.: Environmental chemistry of aminopolycarboxylate chelating agents. Environ. Sci. Technol. **36**(19), 4009–4016 (2002). https://doi.org/10.1021/es025683s
56. Meng, Y., Lu, J., Cheng, Y., Li, Q., Wang, H.: Lignin-based hydrogels: a review of preparation, properties, and application. Int. J. Biol. Macromol. **135**, 1006–1019 (2019). https://doi.org/10.1016/j.ijbiomac.2019.05.198
57. Li, M., Jiang, X., Wang, D., Xu, Z., Yang, M.: In situ reduction of silver nanoparticles in the lignin based hydrogel for enhanced antibacterial application. Colloids Surf. B Biointerfaces **177**, 370–376 (2019). https://doi.org/10.1016/j.colsurfb.2019.02.029
58. Ciolacu, D., Oprea, A.M., Anghel, N., Cazacu, G., Cazacu, M.: New cellulose-lignin hydrogels and their application in controlled release of polyphenols. Mater. Sci. Eng. C **32**(3), 452–463 (2012). https://doi.org/10.1016/j.msec.2011.11.018
59. Wu, L., Huang, S., Zheng, J., Qiu, Z., Lin, X., Qin, Y.: Synthesis and characterization of biomass lignin-based PVA superabsorbent hydrogel. Int. J. Biol. Macromol. **140**, 538–545 (2019). https://doi.org/10.1016/j.ijbiomac.2019.08.142
60. Huang, S., et al.: Facile fabrication and characterization of highly stretchable lignin-based hydroxyethyl cellulose self-healing hydrogel. Carbohydr. Polym. **223**, 115080 (2019). https://doi.org/10.1016/j.carbpol.2019.115080
61. Thakur, S., Govender, P.P., Mamo, M.A., Tamulevicius, S., Mishra, Y.K., Thakur, V.K.: Progress in lignin hydrogels and nanocomposites for water purification: future perspectives. Vacuum **146**, 342–355 (2017). https://doi.org/10.1016/j.vacuum.2017.08.011
62. Ge, Y., Li, Z.: Application of lignin and its derivatives in adsorption of heavy metal ions in water: a review. ACS Sustain. Chem. Eng. **6**(5), 7181–7192 (2018). https://doi.org/10.1021/acssuschemeng.8b01345
63. Jõul, P., et al.: Characterization of Organosolv lignins and their application in the preparation of aerogels. Materials **15**(8), 2861 (2022). https://doi.org/10.3390/ma15082861
64. Mancini, A., et al.: Porosity, bulk density and CaCO3 content of travertines. A new dataset from Rapolano, Canino and Tivoli travertines (Italy). Data Brief **25**, 104158 (2019). https://doi.org/10.1016/j.dib.2019.104158
65. García-Del-Cura, M.Á., Benavente, D., Martínez-Martínez, J., Cueto, N.: Sedimentary structures and physical properties of travertine and carbonate tufa building stone. Constr. Build. Mater. **28**(1), 456–467 (2012). https://doi.org/10.1016/j.conbuildmat.2011.08.042
66. Alesiani, M., Capuani, S., Curzi, F., Mancini, L., Maraviglia, B.: Evaluation of stone pore size distribution by means of NMR. In: Proceedings of the 9th International Congress on Deterioration and Conservation of Stone, pp. 579–585 (2000)
67. Alesiani, M., Capuani, S., Maraviglia, B.: NMR applications to low porosity carbonate stones. Magn. Reson. Imaging **21**(7), 799–804 (2003). https://doi.org/10.1016/S0730-725X(03)00099-7
68. Attanasio, D., Armiento, G., Brilli, M., Emanuele, M.C., Platania, R., Turi, B.: Multi-method marble provenance determinations: the Carrara marbles as a case study for the combined use of isotopic, electron spin resonance and petrographic

data. Archaeometry **42**(2), 257–272 (2000). https://doi.org/10.1111/j.1475-4754.2000.tb00881.x
69. Sassoni, E., Franzoni, E.: Influence of porosity on artificial deterioration of marble and limestone by heating. Appl. Phys. A **115**, 809–816 (2014). https://doi.org/10.1007/s00339-013-7863-4
70. Siegesmund, S., Ruedrich, J., Koch, A.: Marble bowing: comparative studies of three different public building facades. Environ. Geol. **56**, 453–494 (2008). https://doi.org/10.1007/s00254-008-1307-z
71. Yang, W., et al.: Valorization of acid isolated high yield lignin nanoparticles as innovative antioxidant/antimicrobial organic materials. ACS Sustain. Chem. Eng. **6**, 3502–3514 (2018). https://doi.org/10.1021/acssuschemeng.7b03782
72. Giuliani, L., et al.: Assessment and characterization of *Origanum vulgare* essential oil in highly viscous polymeric dispersions for cleaning cultural heritage stone materials. J. Cult. Herit. **77**, 341–350 (2026). https://doi.org/10.1016/j.culher.2025.12.008
73. Meiboom, S., Gill, D.: Modified spin-echo method for measuring nuclear relaxation times. Rev. Sci. Instrum. **29**, 688–691 (1958). https://doi.org/10.1063/1.1716296
74. Galvosas, P., Callaghan, P.T.: Multi-dimensional inverse Laplace spectroscopy in the NMR of porous media. Comptes Rendus Phys. **11**(2), 172–180 (2010). https://doi.org/10.1016/j.crhy.2010.06.014
75. Venkataramanan, L., Song, Y.Q., Hürlimann, M.D.: Solving Fredholm integrals of the first kind with tensor product structure in 2 and 2.5 dimensions. IEEE Trans. Signal Process. **50**(5), 1017–1026 (2002). https://doi.org/10.1109/78.995059
76. Berman, P., Levi, O., Parmet, Y., Saunders, M., Wiesman, Z.: Laplace inversion of low-resolution NMR relaxometry data using sparse representation methods. Concepts Magn. Reson. A Bridg. Educ. Res. **42**, 72–88 (2013). https://doi.org/10.1002/cmr.a.21263
77. Urbańczyk, M., Bernin, D., Koźmiński, W., Kazimierczuk, K.: Iterative thresholding algorithm for multiexponential decay applied to PGSE NMR data. Anal. Chem. **85**, 1828–1833 (2013). https://doi.org/10.1021/ac3032004
78. De Haro, A., et al.: Methodologies for the characterization and identification of natural Atacamite as a pigment in Andean Colonial Painting. Heritage **6**(7), 5116–5129 (2023). https://doi.org/10.3390/heritage6070272
79. Di Carlo, G., et al.: Artificial patina formation onto copper-based alloys: chloride and sulphate induced corrosion processes. Appl. Surf. Sci. **421**(Part A), 120–127 (2017). https://doi.org/10.1016/j.apsusc.2017.01.080
80. Frost, R.L., Reddy, B.J., Keeffe, E.C.: Structure of selected basic copper(II) sulphate minerals based upon spectroscopy: implications for hydrogen bonding. J. Mol. Struct. **977**(1), 90–99 (2010). https://doi.org/10.1016/j.molstruc.2010.05.019
81. Secco, E.A.: Spectroscopic properties of SO_4 (and OH) in different molecular and crystalline environments. I. Infrared spectra of $Cu_4(OH)_6SO_4$, $Cu_4(OH)_4OSO_4$, and $Cu_3(OH)_4SO_4$. Can. J. Chem. **66**(2), 329–336 (1988). https://doi.org/10.1139/v88-057
82. Miller, F.A., Carlson, G.L., Bentley, F.F., Jones, W.H.: Infrared spectra of inorganic ions in the cesium bromide region (700–300 cm^{-1}). Spectrochim. Acta **16**(1), 135–235 (1960). https://doi.org/10.1016/0371-1951(60)80077-X
83. Smith, D.H., Seshadri, K.S.: Infrared spectra of $Mg_2Ca(SO_4)_3$, $MgSO_4$, hexagonal $CaSO_4$, and orthorhombic $CaSO_4$. Spectrochim. Acta A Mol. Biomol. Spectrosc. **55**(4), 795–805 (1999). https://doi.org/10.1016/S1386-1425(98)00206-6
84. Fan, L., Zhang, X.: ATR-FTIR spectroscopic characterization of ferric arsenic-containing colloid and gypsum. Desalin. Water Treat. **153**, 130–135 (2019). https://doi.org/10.5004/dwt.2019.23721
85. Yusuf, M.O.: Bond characterization in cementitious material binders using Fourier-Transform Infrared Spectroscopy. Appl. Sci. **13**(5), 3353 (2023). https://doi.org/10.3390/app13053353
86. Zaffino, C., Guglielmi, V., Faraone, S., Vinaccia, A., Bruni, S.: Exploiting external reflection FTIR spectroscopy for the in-situ identification of pigments and binders in illuminated manuscripts. Brochantite and Posnjakite as a case study. Spectrochim. Acta A. Mol. Biomol. Spectrosc. **136**, 1076–1085 (2015). https://doi.org/10.1016/j.saa.2014.09.132
87. Catelli, E., Sciutto, G., Prati, S., Jia, Y., Mazzeo, R.: Characterization of outdoor bronze monument patinas: the potentialities of near-infrared spectroscopic analysis. Environ. Sci. Pollut. Res. **25**(24), 24379–24393 (2018). https://doi.org/10.1007/s11356-018-2483-3
88. Chio, C.H., Sharma, S.K., Muenow, D.W.: Micro-Raman studies of hydrous ferrous sulfates and jarosites. Spectrochim. Acta A Mol. Biomol. Spectrosc. **61**(10), 2428–2433 (2005). https://doi.org/10.1016/j.saa.2005.02.021
89. Privitera, A., Corbascio, A., Calcani, G., Della Ventura, G., Ricci, M.A., Sodo, A.: Raman approach to the forensic study of bronze patinas. J. Archaeol. Sci. Rep. **39**, 103115 (2021). https://doi.org/10.1016/j.jasrep.2021.103115
90. Hayez, V., Guillaume, J., Hubin, A., Terryn, H.: Micro-Raman spectroscopy for the study of corrosion products on copper alloys: setting up of a reference database and studying works of art. J. Raman Spectrosc. **35**(8–9), 732–738 (2004). https://doi.org/10.1002/jrs.1194
91. Martens, W., Frost, R.L., Kloprogge, J.T., Williams, P.A.: Raman spectroscopic study of the basic copper sulphates: implications for copper corrosion and 'bronze disease.' J. Raman Spectrosc. **34**(2), 145–151 (2003). https://doi.org/10.1002/jrs.969
92. Ospitali, F., Chiavari, C., Martini, C., Bernardi, E., Passarini, F., Robbiola, L.: The characterization of Sn-based corrosion products in ancient bronzes: a Raman approach. J. Raman Spectrosc. **43**(11), 1596–1603 (2012). https://doi.org/10.1002/jrs.4037
93. Debbichi, L., Marco de Lucas, M.C., Pierson, J.F., Krüger, P.: Vibrational properties of CuO and Cu4O3 from first-principles calculations, and Raman and infrared spectroscopy. J. Phys. Chem. C **116**(18), 10232–10237 (2012). https://doi.org/10.1021/jp303096m
94. Liu, Y.: Raman, Mid-IR, and NIR spectroscopic study of calcium sulfates and mapping gypsum abundances in Columbus Crater, Mars. Planet. Space Sci. **163**, 35–41 (2018). https://doi.org/10.1016/j.pss.2018.04.010
95. Ciolacu, D., Cazacu, G.: New green hydrogels based on lignin. J. Nanosci. Nanotechnol. **18**(4), 2811–2822 (2018)
96. Chirea, M., Freitas, A., Vasile, B.S., Ghitulica, C., Pereira, C.M., Silva, F.: Gold nanowire networks: synthesis, characterization, and catalytic activity. Langmuir **27**(7), 3906–3913 (2011). https://doi.org/10.1021/la104092b
97. Spoljaric, S., Salminen, A., Luong, N.D., Seppälä, J.: Stable, self-healing hydrogels from nanofibrillated cellulose, poly(vinyl alcohol) and borax via reversible crosslinking. Eur. Polym. J. **56**(1), 105–117 (2014). https://doi.org/10.1016/j.eurpolymj.2014.03.009
98. Chaudhary, J.P., Kholiya, F., Vadodariya, N., Budheliya, V.M., Gogda, A., Meena, R.: Carboxymethylagarose-based multifunctional hydrogel with super stretchable, self-healable having film and fiber forming properties. Arab. J. Chem. **13**(1), 1661–1668 (2020). https://doi.org/10.1016/j.arabjc.2017.12.034

99. White, R.L.: Variable temperature infrared study of copper sulfate pentahydrate dehydration. Thermochim. Acta **528**, 58–62 (2012). https://doi.org/10.1016/j.tca.2011.11.013
100. Ibrahim, M.N.M., Iqbal, A., Shen, C.C., Bhawani, S.A., Adam, F.: Synthesis of lignin based composites of TiO2 for potential application as radical scavengers in sunscreen formulation. BMC Chem. **13**(1), 17 (2019). https://doi.org/10.1186/s13065-019-0537-3
101. Rashid, T., Kait, C.F., Murugesan, T.: A 'Fourier transformed infrared' compound study of lignin recovered from a formic acid process. Procedia Eng. **148**, 1312–1319 (2016). https://doi.org/10.1016/j.proeng.2016.06.547
102. Kubo, S., Kadla, J.F.: The formation of strong intermolecular interactions in immiscible blends of poly(vinyl alcohol) (PVA) and lignin. Biomacromol **4**(3), 561–567 (2003). https://doi.org/10.1021/bm025727p
103. Benavente, D., Martinez-Martinez, J., Cueto, N., Ordoñez, S., Garcia-del-Cura, M.A.: Impact of salt and frost weathering on the physical and durability properties of travertines and carbonate tufas used as building material. Environ. Earth Sci. **77**, 147 (2018). https://doi.org/10.1007/s12665-018-7339-0
104. Çobanoğlu, İ: Prediction and identification of capillary water absorption capacity of travertine dimension stone. Arab. J. Geosci. **8**(11), 10135–10149 (2015). https://doi.org/10.1007/s12517-015-1902-8

Authors and Affiliations

Valeria Stagno[1,2] · Melania Di Fazio[1] · Laura Giuliani[1] · Rosaceleste Zumpano[3] · Alessandro Ciccola[4] · Elisa Villani[1] · Chiara Genova[2] · Laura Medeghini[1] · Silvia Capuani[2]

✉ Valeria Stagno
valeria.stagno@uniroma1.it

Melania Di Fazio
melania.difazio@uniroma1.it

Laura Giuliani
laura.giuliani@uniroma1.it

Rosaceleste Zumpano
rosaceleste.zumpano@uniroma1.it

Alessandro Ciccola
alessandro.ciccola@uniroma1.it

Elisa Villani
elisa.villani@uniroma1.it

Chiara Genova
chiara.genova@uniroma1.it

Laura Medeghini
laura.medeghini@uniroma1.it

Silvia Capuani
silvia.capuani@cnr.it

[1] Department of Earth Sciences, Sapienza University of Rome, P.le Aldo Moro 5, 00185 Rome, Italy

[2] National Research Council Institute for Complex Systems (CNR-ISC) C/o Physics Department, Sapienza University of Rome, P.le Aldo Moro 5, 00185 Rome, Italy

[3] Department of Chemistry and Drug Technologies, Sapienza University of Rome, P.le Aldo Moro 5, 00185 Rome, Italy

[4] Department of Environmental Biology, Sapienza University of Rome, P.le Aldo Moro 5, 00185 Rome, Italy